Report

Investigation of the nuclear reaction $^{20}\mathrm{Ne}(\mathrm{p},\gamma)^{21}\mathrm{Na}$ in the energy range of astrophysical importance

February 21, 2006

Department:	Physics
Author:	Sascha Falahat
Advisors:	Prof. Dr. M. Wiescher
	Prof. Dr. J. Görres

Abstract

In this report, the nuclear reaction $^{20}Ne(p,\gamma)^{21}Na$ has been investigated in the astrophysical energy region of interest from $E_p = 600\,k$eV to $E_p = 1400\,k$eV. Furthermore, several resonances of the reaction $^{27}Al(p,\gamma)^{28}Si$ have been measured in the energy range of $E_p = 400\,k$eV to $E_p = 1400\,k$eV to determine the calibration and efficiency of the detector setup.
The experiments and corresponding measurements have been performed at the Nuclear Structure Laboratory at the University of Notre Dame (Notre Dame, Indiana 46556, USA) with the KN and JN Van-de-Graaff accelerators. Implanted ^{20}Ne and evaporated ^{27}Al targets have been bombarded with protons and the induced reactions have been investigated. For the γ-spectroscopy measurements, a Ge-detector and a pair of NaI-detectors have been used in several setups.

Contents

List of Figures

List of Tables

Chapter 1

Introduction

1.1 The NeNa-Cycle

In the following; a short introduction to the NeNa-Cycle is given, in which the investigated reaction $^{20}Ne(p,\gamma)^{21}Na$ is plays an important role.

During the hot CNO-Cycle, a "breakout" via the reaction $^{19}F(p,\gamma)^{20}Ne$ can take place, so that ^{20}Ne is produced and the reaction $^{20}Ne(p,\gamma)^{21}Na$ can proceed [1], [2]. Another process which leads to the production of ^{20}Ne is the triple-α-process. Here the reaction $^{16}O(\alpha,\gamma)^{20}Ne$ takes place, after ^{16}O has been produced through the reaction $^{12}C(\alpha,\gamma)^{16}O$. It is worthwhile to note, that both breakout reactions do not compete with the original burning processes, due to small cross sections.
As soon as the produced ^{20}Ne enters an environment in which, compared to the CNO-Cycle, high temperatures occur, proton capture reactions can take place and the reaction cycle shown in figure 1.1 proceeds.

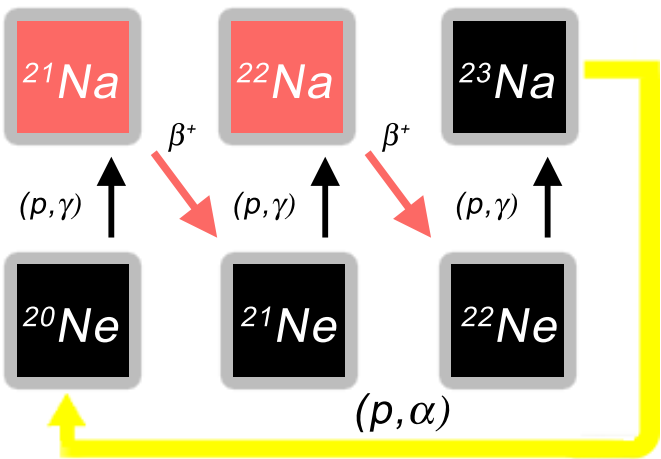

Figure 1.1: The NeNa-Cycle

Another scenario, in which the NeNa-Cycle can take place, is binary star systems, where one star is a white dwarf. This white dwarf has completed the stage of C-burning, whereas the Ne-burning phase has not been initiated yet. At this point, the white dwarf emerges

with an increased amount of Neon, Sodium and Magnesium. As soon as the white dwarf acreets mass from its neighbor star, the NeNa-Cycle can start via interactions caused by the incoming mass.

Analog to the CNO-Cycle, the NeNa-Cycle has several options to take place, depending on the environment (especially the temperature) in which the nuclei are located. After taking the participating decay schemes and half-lives for each isotope into account, it is to point out, that the β^+ decay of ^{22}Na is the slowest with a half-life of 2.6 years.

This is to be considered as a branching point in the NeNa-Cycle, in which the β^+ decay competes with the proton capture of ^{22}Na.

When the temperature in the environment of the NeNa-Cycle high enough, a break-out from the NeNa-Cycle via the reactions $^{23}Na(p,\gamma)$ and $^{23}Mg(p,\gamma)$ can take place. This will happen if proton capture is favored over to the β^+-decay of the nuclei $^{23}Na(p,\gamma)$ and $^{23}Mg(p,\gamma)$. The resulting reaction cycle is known as the MgAl-Cycle.

Rowland et al. have shown in their article from 2004 [4], that a closed NeNa-Cycle is not possible for a temperature range of $T_9 = 0.2 - 0.4\,\mathrm{K}$[1], considering a nova scenario.

The NeNa-Cycle is not playing an important role considering the energy generation within most astrophysical sites. The only exception seem to be Nova explosions with a temperature of $T_9 = 0.2\,\mathrm{K}$ [3].

1.2 The reaction $^{20}Ne(p,\gamma)^{21}Na$ within the NeNa-Cycle

As illustrated before, the reaction $^{20}Ne(p,\gamma)^{21}Na$ is the starting point for the NeNa-Cycle.

In particular, the fact that the proton capture reaction of ^{20}Ne is taking place orders of magnitude less often than the other capture reactions in the NeNa-Cycle, emphasizes the importance of the reaction $^{20}Ne(p,\gamma)^{21}Na$.

When investigating the $^{20}Ne(p,\gamma)^{21}Na$ reaction it is important to focus on the non-resonant direct capture reactions for two reasons (see figure 1.3). First, the stellar scenarios following the NeNa-Cycle implicate temperatures less than 1 MeV. Also there are no resonances with relevant resonance strengths over 1 MeV.

These capture reactions have a relatively low cross section and are difficult to investigate experimentally. However, help does come from a parallel measurement of the resonance at $E_p = 1169$ keV (see figure 1.2) and the determination of its resonance strength, which allows the calculation of the cross section for the non-resonant direct capture reaction.

Previous results for the resonance strength and the cross section have been published by Tanner [5] (1959), Rolfs et al. [6] (1974) and Stech [7] (2004) (see table 1.1).

Compared to our experiments, the cited publishers used different target systems (gas targets, evaporated targets, etc.) and different methods to determine e.g. cross sections and reaction rates.

[1] $T_9 = 10^9 K$

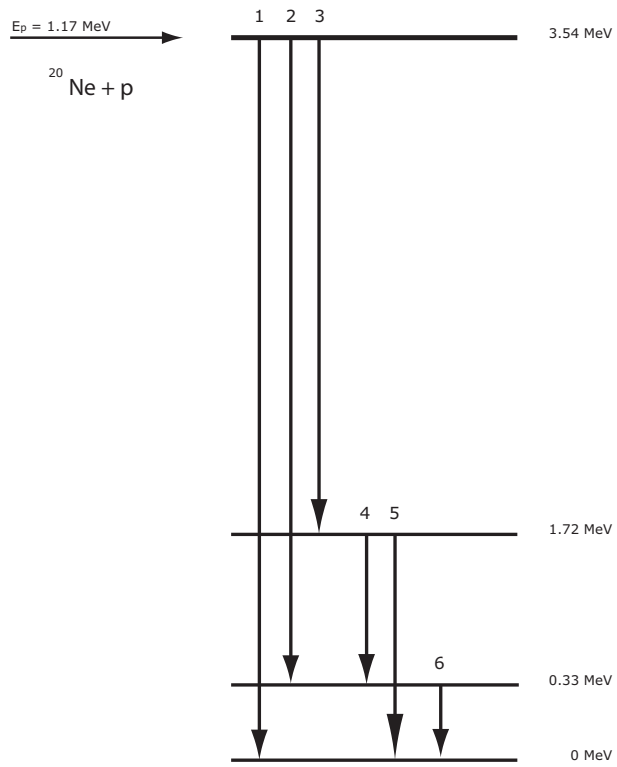

Figure 1.2: The simplified decay scheme of ^{21}Na at a resonance energy of $E_p = 1169\,k$eV. The numbers over the arrows are for the calculation of summing corrections, which will be calculated in Appendix A.

Reference	Energy E_p (keV)	Cross section (μb)	$\omega\gamma_{1169}$(eV)
Tanner [5]	1102	0.49 ± 0.10	1.13
Rolfs et al. [6]	1050	0.63 ± 0.7	1.13
Stech [7]	925	0.28 ± 0.03	1.13
	925	0.29 ± 0.03	1.13
	750	0.11 ± 0.02	1.13
	600	0.038 ± 0.007	1.13
	500	0.012 ± 0.002	1.13

Table 1.1: Results of previous experiments for the direct capture reaction (DC → 2425) below the 1169 keV resonance. The different values for $E_p = 925\,k$eV of E.Stech [7] result from different experimental setups.

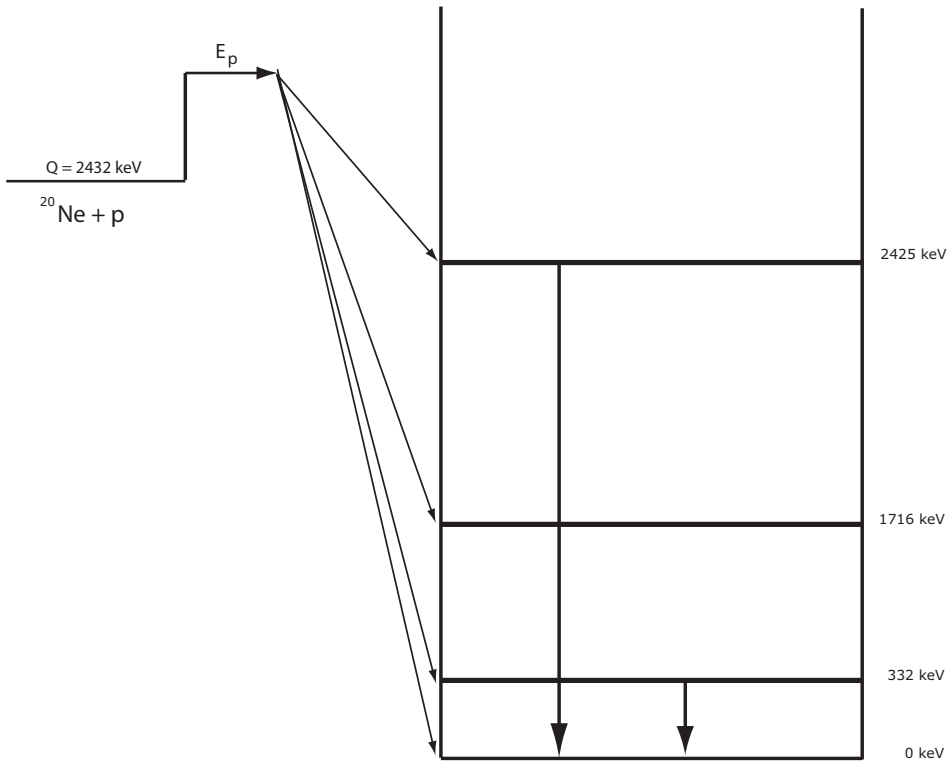

Figure 1.3: The simplified decay scheme of ^{21}Na for the direct capture reaction.

Chapter 2

Experimental setups and procedures

2.1 Accelerators and beam optics

2.1.1 Accelerators

The protons beams used for the (p, γ)-reactions have been produced with the KN and JN accelerators (see figure 2.1). The proton beams have been directed and focused on solid state targets.

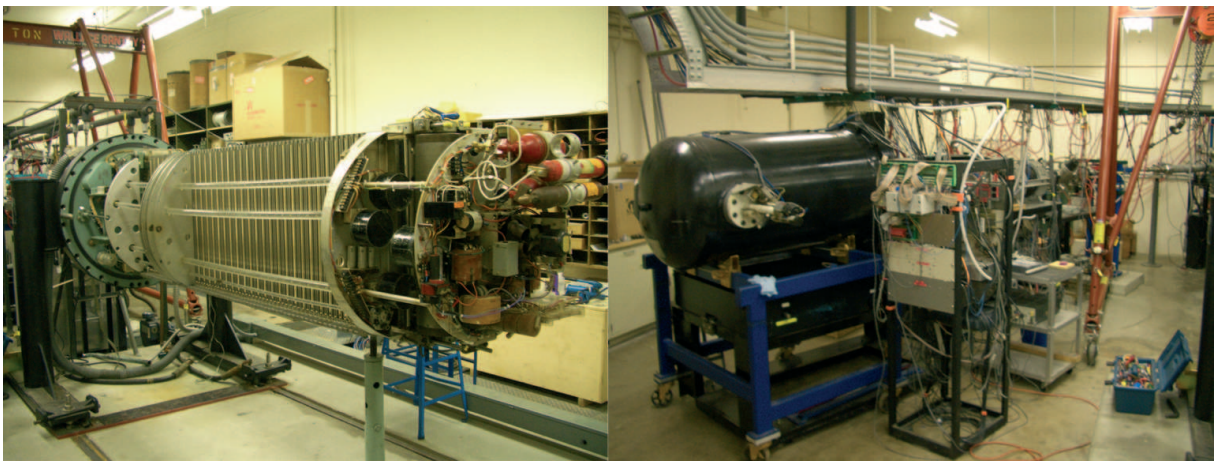

Figure 2.1: KN (left, with open tank) and JN (right, with closed tank) Accelerators

The reasons for the use of two accelerators is the fact that the JN accelerator is not capable of generating terminal voltages above 1 MV, while the KN was not capable of generating terminal voltages below 0.7 MV.

2.1.2 Beam optics

After generating the beam, the beam is guided through an analyzing magnet whose magnet field deflects the beam for a well defined energy (depending on the magnet field) into the target room. After entering the target room, the proton beam enters the so called switching

magnet, which deflects the beam into the different beamlines. In our case the beam was deflected into the (p, γ)-beamline, which is at 0°.

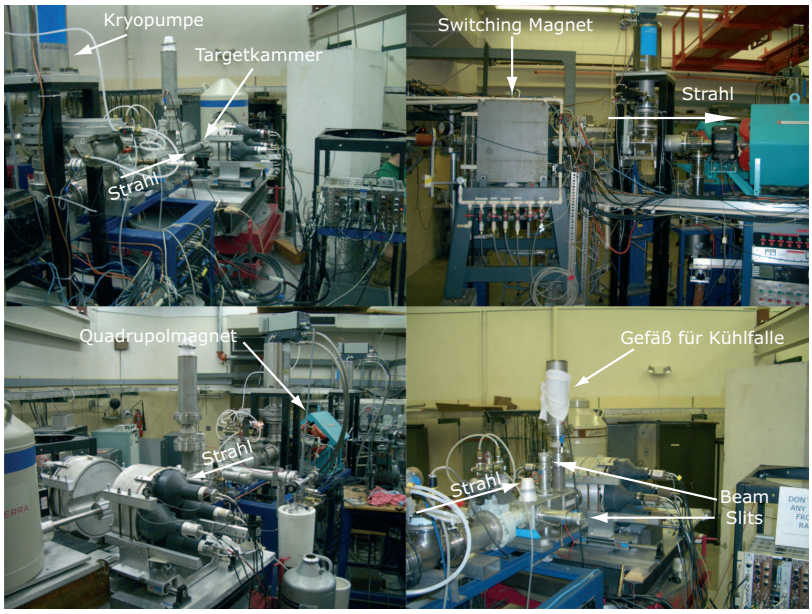

Figure 2.2: The (p, γ)-beamline from different perspectives

The beam is then focused and directed to the target by means of quadrupole magnets and steering elements. The target was mounted at the end of a target chamber containing a cold trap (see figures 2.2 and 2.3).
For the first experiment an aluminium pipe and target holder were used, on which the target was mounted at 0° with respect to the beam. The second experiment also included a 45° setup, where the pipe was replaced by an aluminium-brass pipe and the target holder was replaced by a special target holder, which held the target at 45° with respect to the beam.
To ensure, that the beam is hitting the target in the right position, the beam current was read from beam slits which are mounted in the beamline. Before mounting the target, a quartz window was mounted, behind which a CCD camera was positioned. With the quartz window and the CCD camera, it was possible to position the beam while using a monitor in the control room of the accelerators (see figure 2.4).

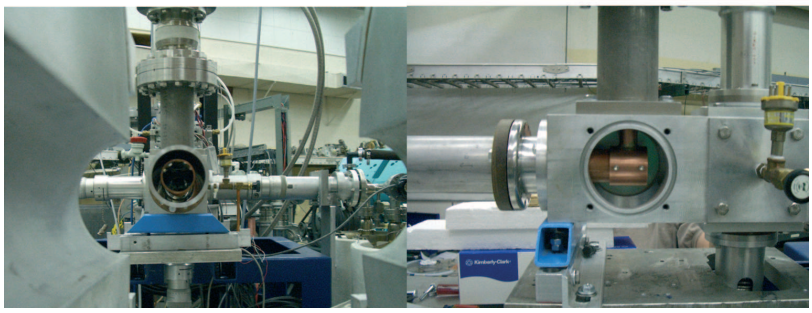

Figure 2.3: Drawing of the target chamber and pictures of the open target chamber. The pipe within the beamline pipe is the cold trap which is connected to a liquid nitrogen dewar.

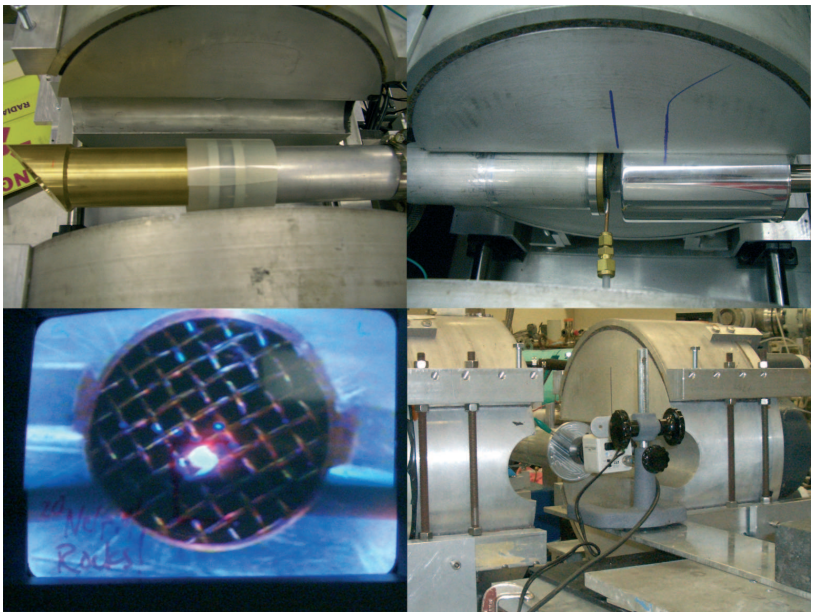

Figure 2.4: At the top : both target chambers (0° right, 45° left), whereas the 0° chamber has the mounted target with the cooling water connections. At the bottom : the CCD camera (right) and the picture on the screen (left) in the control room.

2.2 Targets

Two ^{20}Ne solid state targets were used. The targets were produced in Germany at the Ruhr-Universität Bochum (in the following named as Bochum Target)and the Universität Münster (in the following named as Münster Target).
The Bochum Target was produced by implanting ^{20}Ne with a 200 keV accelerator into a Cu-Ni-plate (thickness $\approx 1\,m$m)(see figure 2.5).
The Münster Target was also produced by implantation, whereas Ta of a thickness of 0.254 mm was used as a backing material.
A disadvantage of using implanted targets is the unknown implantation depth as well as the thickness of the target material.
The solution for the problem was the measurement of the $^{20}Ne(p,\gamma)^{21}Na$-resonance at an energy of $E_p = 1169\,k$eV. The Full Width Half Maximum (FWHM) of the yield curve gives the target thickness in energy units (see figure 2.6).

Figure 2.5: The Bochum Target before (left) and after the exposure to the proton beam (right).

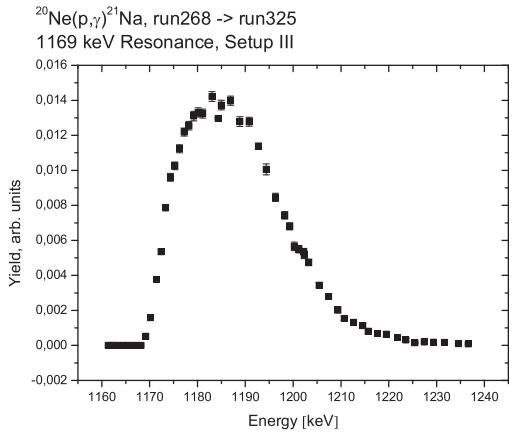

Figure 2.6: Illustrated is the yield curve for the $^{20}Ne(p,\gamma)^{21}Na$ resonance at $E_p = 1169\,k$eV.

2.3 Detectors

In each of the two experiments, a Ge and a pair of NaI detectors were used.

The reason for the use of both detector types was the investigation of the suppression of Cosmic radiation and the radiation caused by Compton scattering.

Therefore, the NaI detectors were used as veto detectors in coincidence and anti-coincidence mode with the Ge detector.

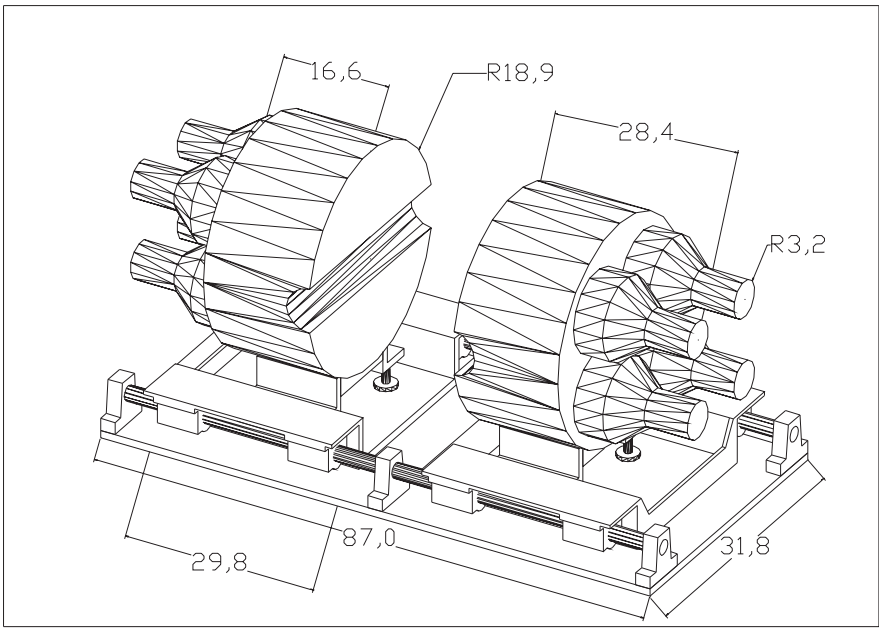

numbers are in cm
by P.J. LeBlanc

Figure 2.7: Drawing of the NaI detectors on movable plates.

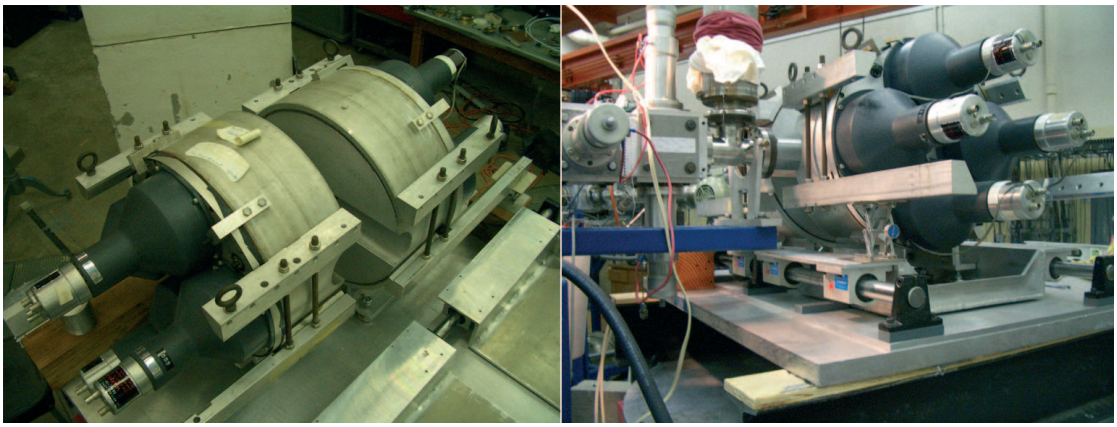

Figure 2.8: Picture of the NaI detectors on (right) and without (left) movable plates.

2.3.1 Detector setups

Three different setups were used. Setup I was used in both experiments, while Setup II and Setup III were only used in the second experiment.

Setup I

In setup I, the Ge detector and target have been enclosed by the NaI detectors. The Ge detector was positioned at an angle of 0° with respect to the target, at two distances, 14.351 mm and 50.698 mm (see figure 2.9).

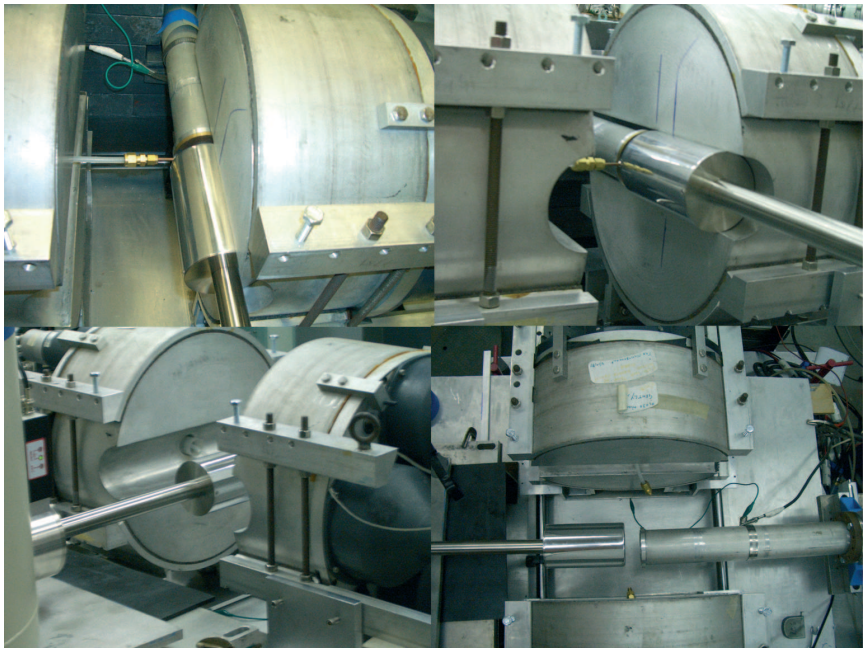

Figure 2.9: Setup I, illustrated from different perspectives. For visualization the NaI detectors do not enclose the target and the Ge detector.

To simplify the opening and movement of the NaI detectors, the detectors have been placed on two movable plates (see figures 2.7 and 2.8).
The Ge detector was moved first by hand and afterwards also placed on a movable plate. One problem that occurred, was the fact that the Ge detectors had different radii. For example, the radius of the Canberra detector cap was too big to let the NaI detectors enclose the target and the Ge detectors completely. Consequently during the first experiment, there was a gap of 1.5 cm between the NaI detectors which had negative effects on the efficiency of the setup.

Setup II

For the second setup, the NaI detectors were moved so that the target was at the end of the NaI detectors. The Ge detector was placed at 0° with respect to the target. Again, different detector to target were used. (see figure 2.10).

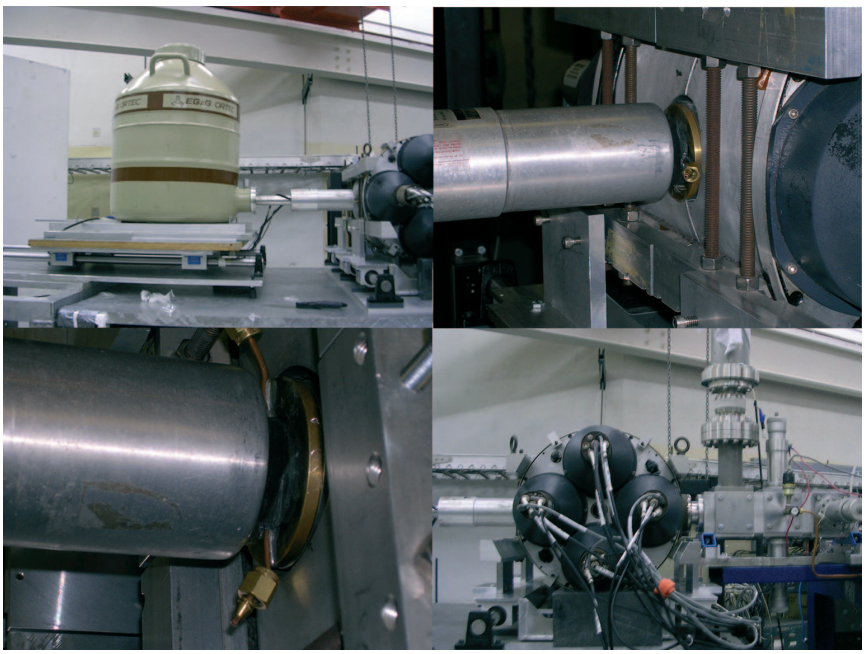

Figure 2.10: Setup II, illustrated from different perspectives.

Setup III

Setup III follows in principle Setup II, where in comparison to Setup II a 45° target chamber made out of brass was mounted at the end of the beamline. The mounting of the 45° chamber allowed the beam to hit the target at an angle of 45°. Correspondingly, the Ge detector was rotated and operated at different distances to the target (see figure 2.11).

2.3.2 Coincidence - anti-coincidence coupling of the detectors

The reason for operating two different detector types is because the direct capture reactions under investigation are difficult to observe. Therefore any suppression of background is helpful. To realize a background suppression, the NaI detectors have been used as *veto-detectors*.

Suppression of Cosmic radiation

To suppress the Cosmic radiation, the following physical train of thoughts was imposed. Whenever a particle from the Cosmic radiation hits the NaI detector, it usually has enough energy to hit also the Ge detector. With a typical NaI detector response time of 500 ns, the signal caused by the particle from the Cosmic radiation is detected by the NaI and Ge detectors in principle at the same time. This leads to the need for a anti-coincidence coupling of the Ge and NaI detector. To seperate signals coming from Cosmic radiation and other signals, the typical energy loss of the particle can be calculated and therefore a threshold can be implemented [10].

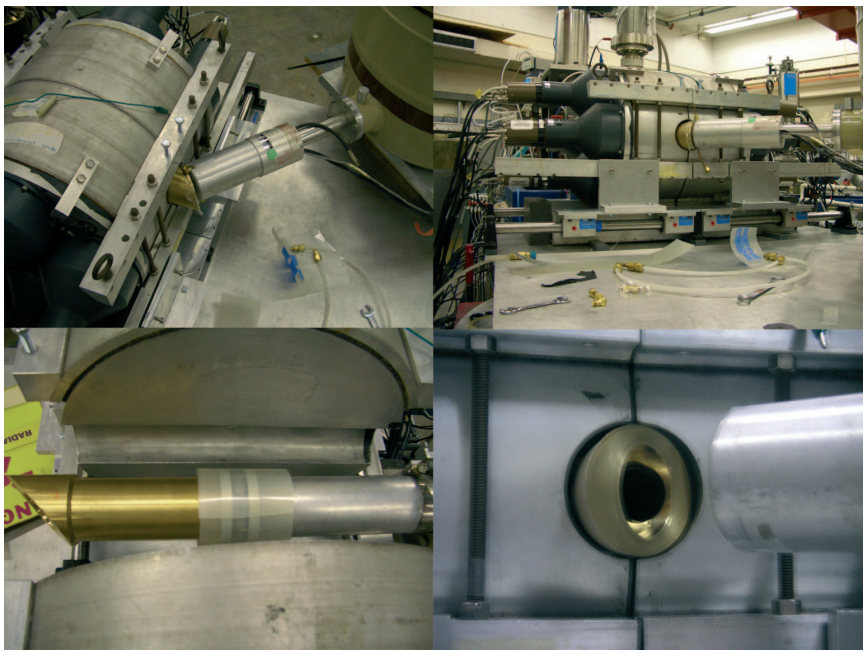

Figure 2.11: Setup III, illustrated from different perspectives.

Suppression of Compton radiation

For the suppression of the Compton radiation, a coupling of both detectors with a well defined time window is needed. The time window is to be opened by the NaI detectors, and if in this time window the Ge detectors detects a signal, the signal is rejected [8].

2.4 Electronics and Data Acquisition

For both experiments, different electronics setups were used, with the shortcomings of the first electronics setup have been partially corrected in the second electronics setup.

2.4.1 Electronics setup for the 1st experiment

The energy signal of the Ge detector was directly processed to a Analog-Digital-Converter (ADC), while the timing signal was given to two separate Time to Amplitude Converters (TAC), after passing a logic unit and amplifiers. The TAC´s have been used to create time windows, which were needed for the suppression of the Cosmic radiation and the Compton radiation.
The photomultiplier bases of the NaI detectors were not able to generate a timing signal, so that at the same time the energy signal was used as a timing signal.
The signal of each of the 8 photomultipliers has been relayed to a 16-Channel-Amplifier. For each of the of NaI detectors the signals were summed, giving one signal for each NaI detector This signal was divided and fed into a Constant Fraction Module, which was used as the threshold module for the suppression of the Cosmic radiation. Then the signal was relayed to one of the TAC´s, to close the specific time window.
The signal of each NaI detector was amplified and delayed through a Delay Line Amplifier.

Subsequently, the signal was passed to an ADC, after being processed through a Linear Gate Stretcher. The same signal was also converted into a timing signal with a Timing Single Channel Analyzer (Timing SCA) , which was used as the stop signal for the time window of the Compton suppression.
In the first experiment, six different voltage supplies were used to power the photomultipliers. However, it was found that this was not very practical due to the individual gain shifts of the photomultipliers, which complicated the gain matching required for the summing of the signals.
The correction of the gain shift has been accomplished with a ^{137}Cs source. Directly after the 16 channel amplifier, the Cs signal was relayed to a Multi-Channel Analyzer (MCA). To correct the gain shift the amplification was adjusted for each photomultiplier, so that the 662 keV line was processed and displayed in the same channel for each photomultiplier.

2.4.2 Electronics setup for the 2nd experiment

For the 2nd experiment, the previously used photomultiplier bases were replaced with new ones, which have a integrated pre-amplifier. Therefore, the pre-amplifier signal could be used as an energy signal, while the anode signal could be used as the timing signal.
Furthermore, the voltage supplies have been replaced by one 16 channel voltage channel from CAEN. This turned out to be an enormous advantage, because this unit could be controlled via a personal computer in the control room.
It was found that the pre-amplifier signal of the NaI detectors could not be processed properly with the previously used sum amplifier. Indeed, the sum amplifier inverted the incoming signals, but this caused problems with the incoming signals of the pre-amplifiers. The consequence was that the sum amplifier had to be replaced with two different sum amplifiers, which also allowed the generation of an separated energy signal for each NaI detector.
The Ge-detector of the 1st experiment (Canberra detector) was replaced by a similar, older detector (OSU detector), whereas the same electronics setup for the Ge detectors has been used. The advantage of using the OSU detector was that the OSU detector has a smaller aluminium cap and therefore the NaI detectors could fully enclose target and Ge detector (see figures 2.12 and 2.13).

2.4.3 Data acquisition

For both experiments, the "FAST" data acquisition system was used. Here the signals have been relayed directly from the ADC´s to the computer.
The difference between the two experiments was the use of seven ADC´s in the 2nd experiment instead of using four ADC´s during the 1st experiment. Figures 2.12 and 2.13 show which ADC processed which information.

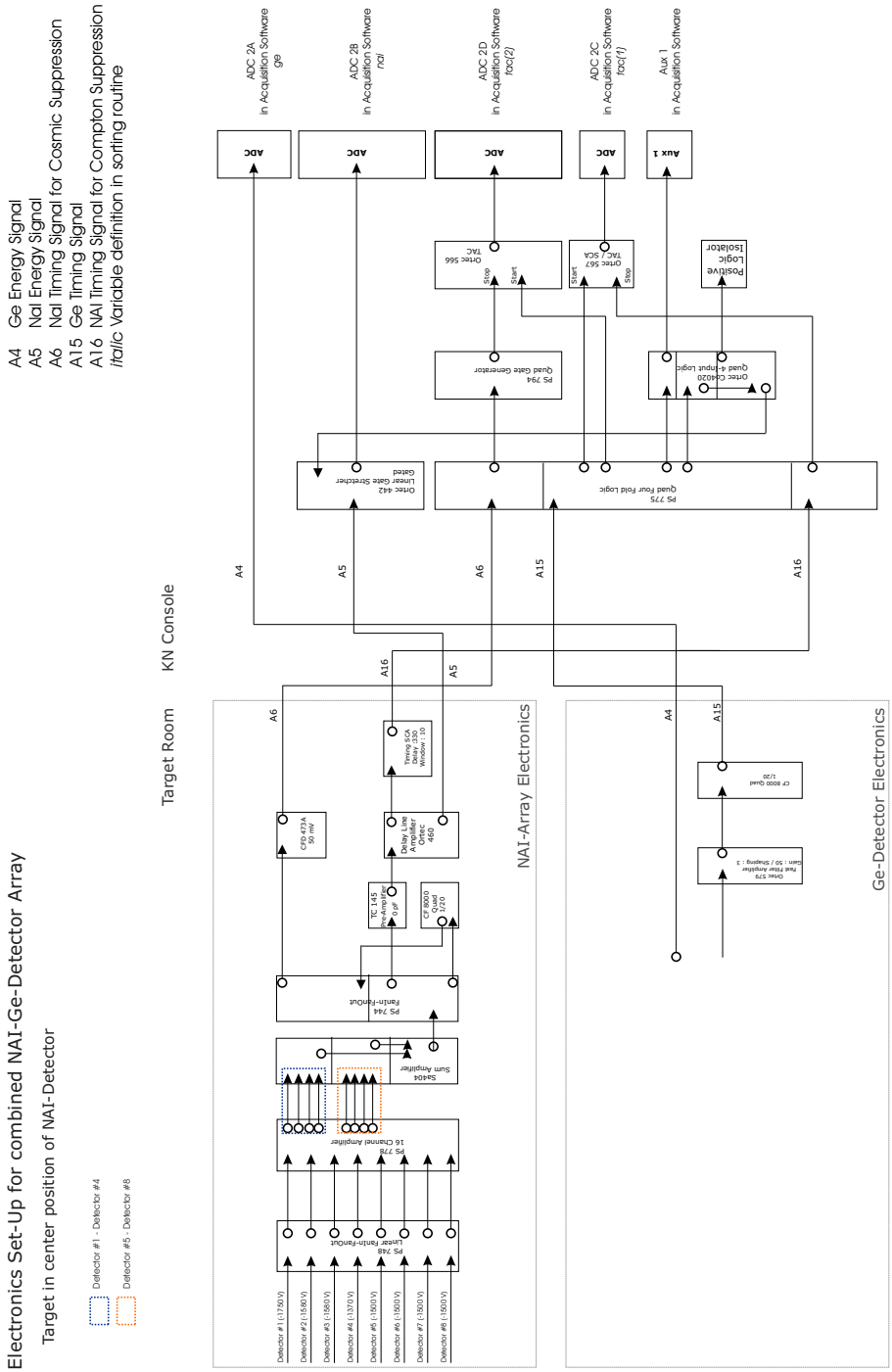

Figure 2.12: The electronics setup for the 1st experiment

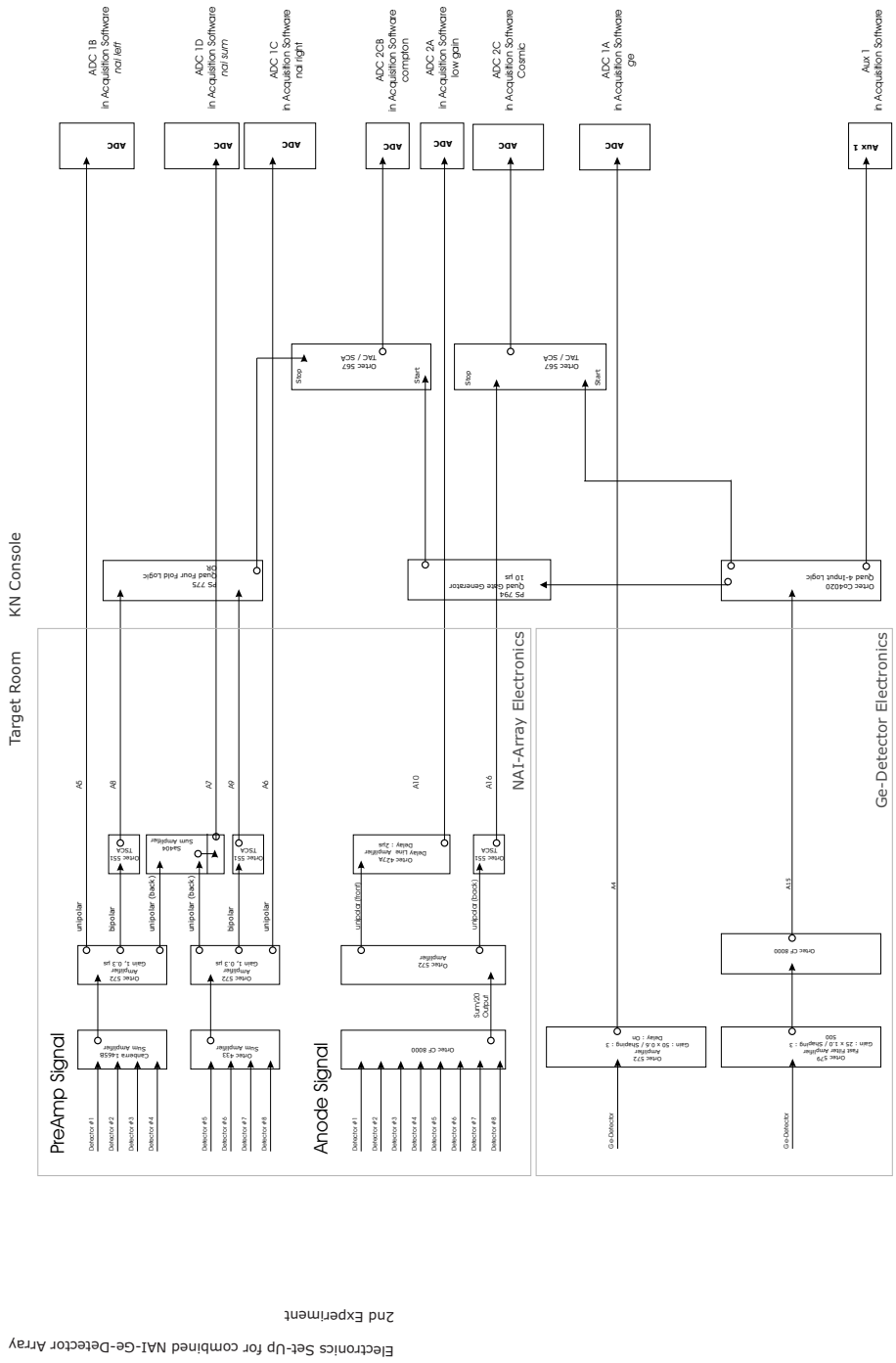

Electronics Set-Up for combined NAI-Ge-Detector Array
2nd Experiment

Figure 2.13: The electronics setup for the 2nd experiment

2.5 Experimental procedures

The experimental procedures for both experiments were very similiar.
Because the detector efficiency of each detector setup is essential for the determination of the physical parameters, the determination of the efficiency has been performed with two different methods for each detector setup.
First, calibrated radioactive sources were used to determine the efficiency in an energy range up to 1.4 MeV. The sources were mounted on the same target holder that was also used during the experiments. Also, the position in which they have been mounted was the same in which the real target was mounted. This has been done to realize an accurate reproduction of the experimental conditions.
To determine the detector efficiency in an energy range higher than 1.4 MeV, the nuclear reaction $^{27}Al(p,\gamma)^{28}Si$ has been measured, which results in radiation of energies up to 11 MeV during the de-excitation of ^{28}Si.
The reason for measuring this reaction is because it is a well documented reaction [11], [12], [13]. Also, the fact that this reaction results in decay schemes, which allow an efficiency determination over an wide energy range, played an important role.
The reaction $^{27}Al(p,\gamma)^{28}Si$ was primarily measured at the resonance energies $E_p = 406\,k$eV, $E_p = 505\,k$eV and $E_p = 992\,k$eV.
During the 1st experiment, the $^{20}Ne(p,\gamma)^{21}Na$ reaction could not be measured as detailed as assumed. Reason for that was the fact, because primarily beam guiding and beam production had problems. Also, it was found that the beamline was not aligned correctly, which led to additional problems.
As mentioned before, problems occurred as a consequence of the gain shift of the photomultipliers of NaI detectors, which could be solved partly with a increased electronic and practical effort.
Another problem during the first experiment was the gap between the two NaI-detectors, which could not enclose target and Ge detector completely, which decreased the overall efficiency.
Of the previously mentioned detector setups, only setup I could be realized in the 1st experiment.
For the 2nd experiment all three detector setups were realized. Also, mechanical and electronic elements were optimized between the two experiments. Furthermore, the beamline and the JN accelerator have been realigned.
Setup III caused a problem concerning the beam alignment. There was no quartz window available, which made a determination of the beam position possible. A consequence was that the beam occassionally hit the target holder or the the target chamber. A contamination of two aluminium targets was also a consequence (see figure 2.14).
In both experiments, the distance between target and Ge-detector has been varied, to determine the effects of summing on the detector efficiency.

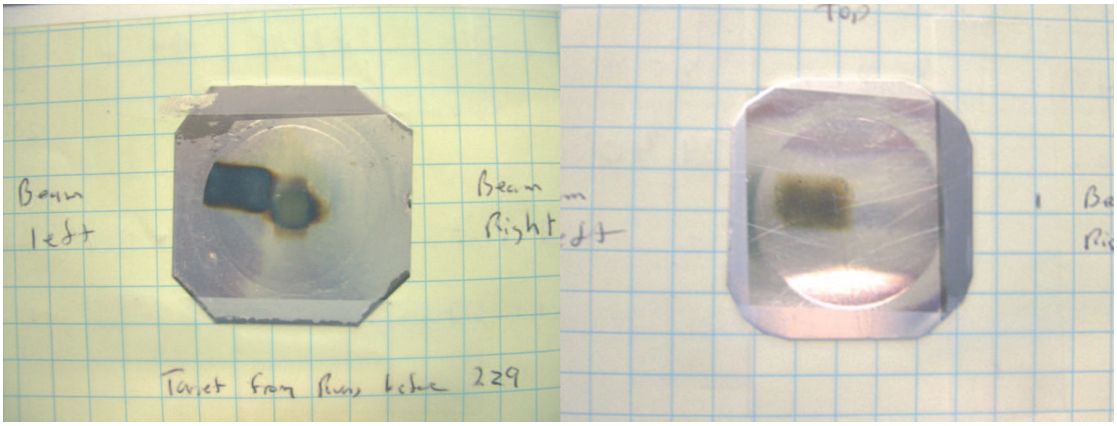

Figure 2.14: Illustrated are the contaminated aluminium targets

Chapter 3

Measurement and calculation of detector characteristics

3.1 Energy calibration

The method for the energy calibration was the combined use of radioactive sources and the measurement of several $^{27}Al(p,\gamma)^{28}Si$ resonances (see table 3.1).

Table 3.1: Listed are the for calibration purposes used sources and $^{27}Al(p,\gamma)^{28}Si$ resonances

$^{27}Al(p,\gamma)^{28}Si$ (keV)	Sources
406	$^{44}Ti \rightarrow^{44} Sc \rightarrow^{44} Ca$
505	^{56}Co
992	^{60}Co
	^{133}Ba
	^{137}Cs

The resonances of $^{27}Al(p,\gamma)^{28}Si$ had to be used, since the radioactive sources allowed only a calibration up to 2.5 MeV.
Furthermore, it is worthwhile to note that doppler shifts and recoils impact the calibration, since the detector sees shifted energies.
A quantity for the quality of the calibration is given by the deviation of calculated channel number from the measured channel number.
Because of the use of four different detectors, four different energy calibration have been performed.

3.1.1 Calibration of the Canberra detector

Five radioactive sources with a total of 13 observable γ-lines have been used. A linear fit of the energy-channel relation was performed (see figure 3.1).
For the Canberra detector, also the $E_p = 992\,k$eV resonance of $^{27}Al(p,\gamma)^{28}Si$ and teh corresponding single and double escape peaks of the transitions have been used.
The correction of doppler shift and recoil effects has been applied via the equation :

$$
\begin{aligned}
E_{Spectra} &= E_\gamma + E_{Doppler} + E_{Recoil} \\
&= E_\gamma + E_\gamma \frac{\sqrt{2m_p E_p}}{m_{^{28}Si}} cos\phi + \frac{E_\gamma}{2m_{^{28}Si}}
\end{aligned}
\tag{3.1}
$$

To reach an accurate calibration in all energy ranges, the measurements of with the radioactive sources and the reaction $^{27}Al(p,\gamma)^{28}Si$ have been combined and a combined fit function was calculated (see figure 3.1).

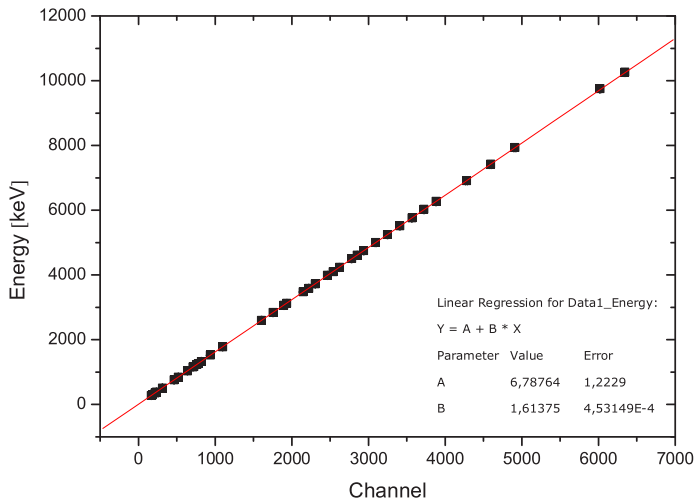

Figure 3.1: Calculated fit function of the combined data points for the Canberra detector.

The quality of the combined fit function can be seen when the ratio between the calculated and measured channels are displayed against the energy. The maximum deviation is 0.4% (see figure 3.2).

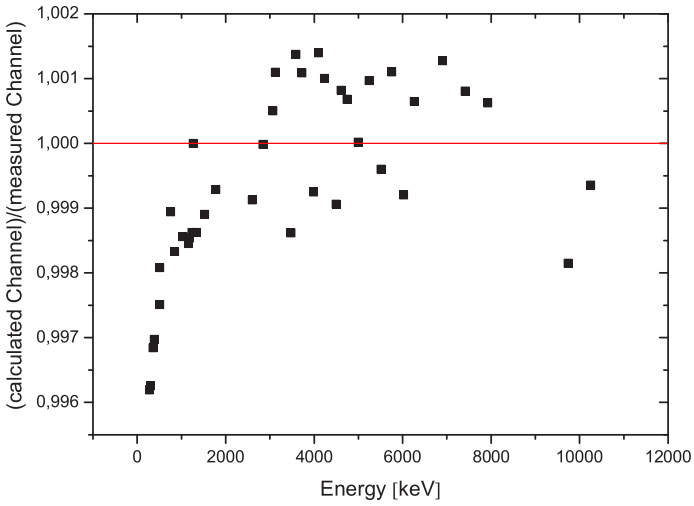

Figure 3.2: Illustration of the quality of the energy calibration for the Canberra detector.

3.1.2 Calibration of the OSU detector

The OSU detector calibration followed the same procedure as the Canberra detector.

Additionally, the experimental data of the reaction $^{27}Al(p,\gamma)^{28}Si$ at the resonance energy $E_p = 406\,k\text{eV}$ has been measured.

For the energy calibration, a maximum deviation of 0.3% between the calculated and measured channel numbers has been calculated (see figures 3.3 and 3.4).

3.1.3 Calibration of the NaI detectors

Due to the low energy resolution of NaI detectors as compared to the Ge detectors, a detailed energy calibration could not be performed. However, the radioactive source were mounted in the center of the NaI detectors, which allowed an energy calibration of each NaI detector and the sum of the two NaI detector signals. This, along with the balance amplification, was important for the experiments, because it helped to detect an correct gain shifting.

The energy calibration for the NaI detectors has not been calculated in detail, since the energy information delivered by the NaI detectors is not important for the analysis of the measurements (see figures 3.5, 3.6 and 3.7).

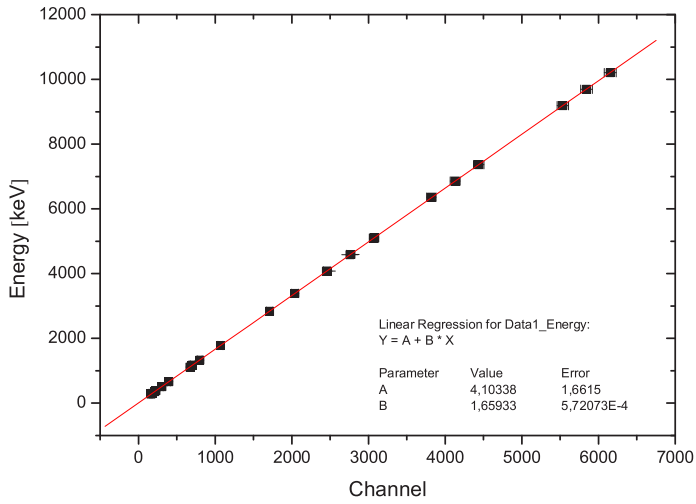

Figure 3.3: Calculated fit function for the combined data points and measurements of the radioactive sources and the reaction $^{27}Al(p,\gamma)^{28}Si$ for the OSU detector.

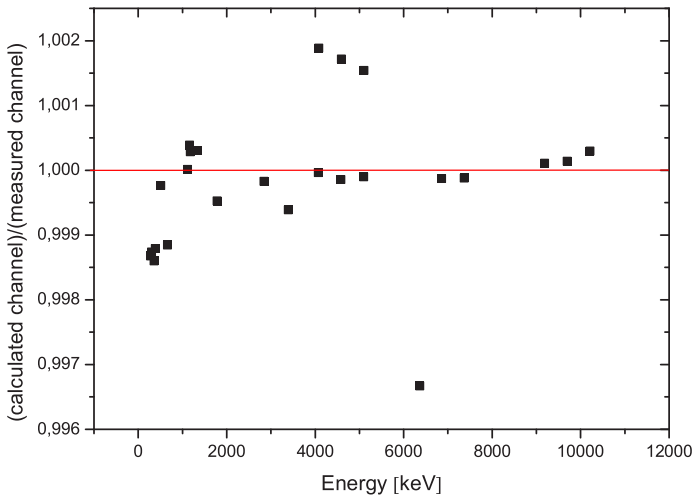

Figure 3.4: Illustration of the quality of the energy calibration for the OSU detector

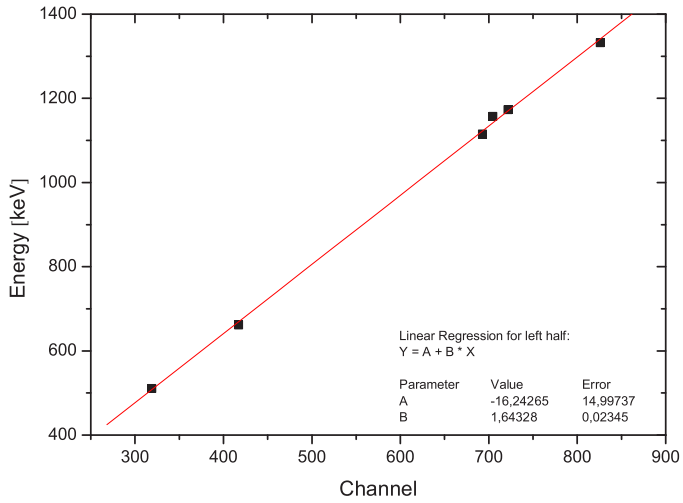

Figure 3.5: Calibration of the *left* NaI detector

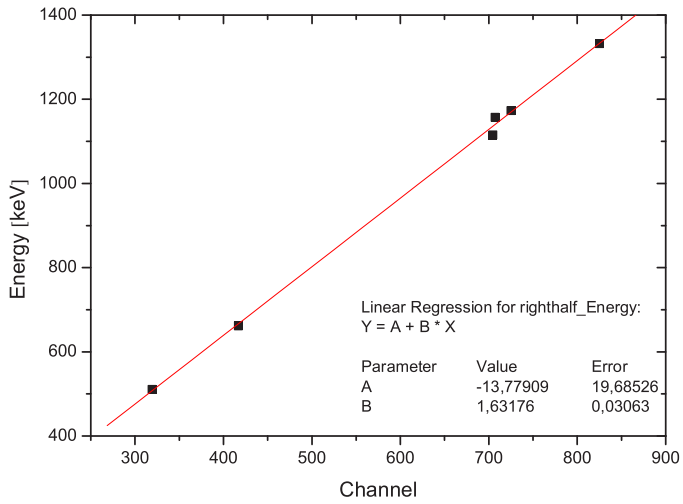

Figure 3.6: Calibration of the *right* NaI detector

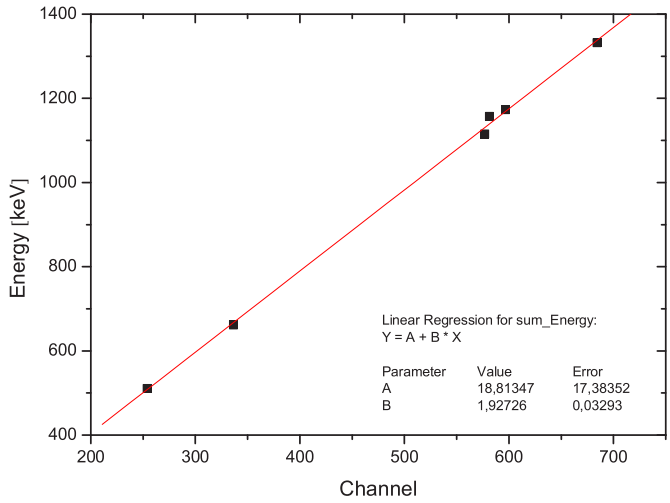

Figure 3.7: Calibration of the sum signal of both NaI detectors

3.2 Detector efficiency

3.2.1 Method for the determination of the detector efficiency

The detector efficiency is dependent on the detector properties and the geometry between detector and radiation source. For these experiments, it was necessary to apply different methods to get an exact efficiency determination for an energy range of 0 - 12 MeV. It was also necessary to calculate the summing corrections for the measured resonances. Finally the effects of Compton and Cosmic radiation suppression have been studied.

Efficiency calculation with radioactive sources

To determine the detector efficiency, it is urgent to know the exact number of decays or reactions which have been taking place. In particular, this number is known for radioactive standard sources, where the activity is known very well.
For an energy range up to 1332.49 keV, radioactive standard sources have been available, which have been used for both Ge detectors.
To measure the efficiency, the sources were mounted in the same position as the target was placed during the experiment. First, the activity at measurement date was calculated:

$$A_{measure} = A_0 e^{-\lambda t} \tag{3.2}$$

where

$$\lambda = \frac{ln2}{t_{1/2}} \tag{3.3}$$

In the above relations λ is the life time, t the number of days between measurement and production date and A_0 the activity at creation date. Subsequently, the number of emitted photons was calculated with the following equation :

$$S = A_{measure} \times \Delta t \times BR \tag{3.4}$$

Here Δt is the measurement time while BR is the branching ratio of the specific transition. With N as the number of the detected events, the efficiency can be calculated as following:

$$\begin{aligned} \epsilon &= \frac{N}{S} \\ &= \frac{N}{A_{measure} \times \Delta t \times BR} \end{aligned} \tag{3.5}$$

Another parameter is the mass absorption due to the Ta and Cu-Backing which was simulated with mounted Ta and Cu-disks of the same thickness. The number of detected events has to be corrected:

$$N = N_0 \times I/I_0 \tag{3.6}$$

Therefore :

$$\begin{aligned}\epsilon &= \frac{N}{S} \\ &= \frac{N}{A_{measure} \times \Delta t \times BR} \\ &= \frac{N_0 \times I/I_0}{A_{measure} \times \Delta t \times BR}\end{aligned} \tag{3.7}$$

A detailed description for the mass absorption is given in Appendix B.

Efficiency calculation with the reaction $^{27}Al(p,\gamma)^{28}Si$

For the energy range in which the accelerators have been operated, the reaction $^{27}Al(p,\gamma)^{28}Si$ has several resonances. The compound nucleus decays over several cascades, which emits γ-radiation over an energy range between $E_\gamma = 1.8\,M$eV and $E_\gamma = 12\,M$eV. This can be utilized to determine the efficiency in the complete energy range. Also, the cross section of the reaction is large, therefore the measurements could be performed in a reasonable time.

For the first experiment the resonance at $E_p = 992\,k$eV was measured. First, the edges of the resonances have been measured. This means, that at an energy lower than the resonance energy one starts and raises the energy in e.g. 1 keV steps. Thereby one observes the number of events for the strongest γ-line. For ^{28}Si, this is the first excited state, which emits a photon with an energy of 1178 keV by decaying exclusively into the ground state. By dividing the number of events by the collected charge, one can calculate the Yield.

$$Y = \frac{N}{Q} \tag{3.8}$$

Under specific conditions, corrections based on relatively large dead times are necessary, but that was not the case for these measurements.

The detector efficiency was then calculated by normalizing to the transition $E_i = 1778\ k$eV $\rightarrow$ $E_f = 0\ k$eV . The relative efficiency is then :

$$\epsilon_{rel}^{\text{uncorrected}}(\Delta E_{if}) = \frac{N_i}{(I/I_0)_{total} \times BR \times N_{37}} \tag{3.9}$$

The index *uncorrected* refers to the calculations which do not include summing corrections (see tables 3.2, 3.3, 3.4 and 3.5).

Table 3.2: Example data set for the $^{27}Al(p,\gamma)^{28}Si$ resonance at $E_p = 992\,keV$, with a distance of $1.44\,cm$ between detector cap of the Canberra detector and the end of the the target holder.

i	E_i (keV)	E_f(keV)	ΔE_{if} (keV)	ϵ_{tot}	$(I/I_0)^{Ta}_{gesamt}$	BR	ϵ_{rel}	$\Delta\epsilon_{rel}$
1	12542	1778	10764	0.0471	0.8565	0.7500	0.0927	0.0006
2	12542	4617	7925	0.0460	0.8676	0.0490	0.2870	0.0042
3	12542	6276	6266	0.0459	0.8737	0.0240	0.2347	0.0055
6	12542	7799	4743	0.0468	0.8784	0.0970	0.3218	0.0032
7	12542	7933	4609	0.0469	0.8787	0.0420	0.4717	0.0059
8	12542	9417	3125	0.0501	0.8790	0.0090	0.5777	0.0140
9	12542	9479	3063	0.0504	0.8790	0.0130	0.6521	0.0124
25	7799	1778	6021	0.0459	0.8747	0.6500	0.2755	0.0036
27	7799	6276	1523	0.0606	0.8539	0.3400	1.1615	0.0103
33	6276	1778	4498	0.0471	0.8789	0.8820	0.3446	0.0045
36	4617	1778	2839	0.0512	0.8776	1.0000	0.5753	0.0054
37	1778	0	1778	0.0580	0.8627	1.0000	1.0000	0.0018

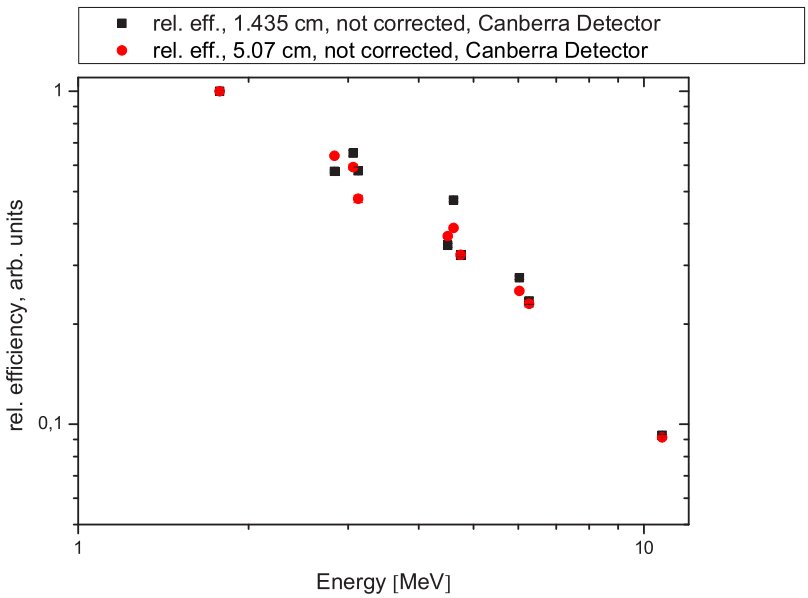

Figure 3.8: Relative efficiency of the Canberra detector for different distances, no summing corrections.

Table 3.3: Calculated values for the relative efficiencies at different distances and energies, Canberra detector, no summing corrections.

E_γ	$\epsilon^{uncorrected}_{1.435cm}$	$\Delta\epsilon^{uncorrected}_{1.435cm}$	$\epsilon^{uncorrected}_{5.07cm}$	$\Delta\epsilon^{uncorrected}_{5.07cm}$
1778	1.0000	0.00180	1.0000	0.00172
2839	0.5753	0.00540	0.6401	0.00544
3063	0.6521	0.01237	0.5924	0.01126
3125	0.5777	0.01399	0.4755	0.01213
4498	0.3446	0.00451	0.3677	0.00445
4609	0.4717	0.00585	0.3891	0.00508
4743	0.3218	0.00318	0.3227	0.00304
6021	0.2755	0.00364	0.2514	0.00332
6266	0.2347	0.00546	0.2303	0.00517
10764	0.0927	0.00061	0.0914	0.00058

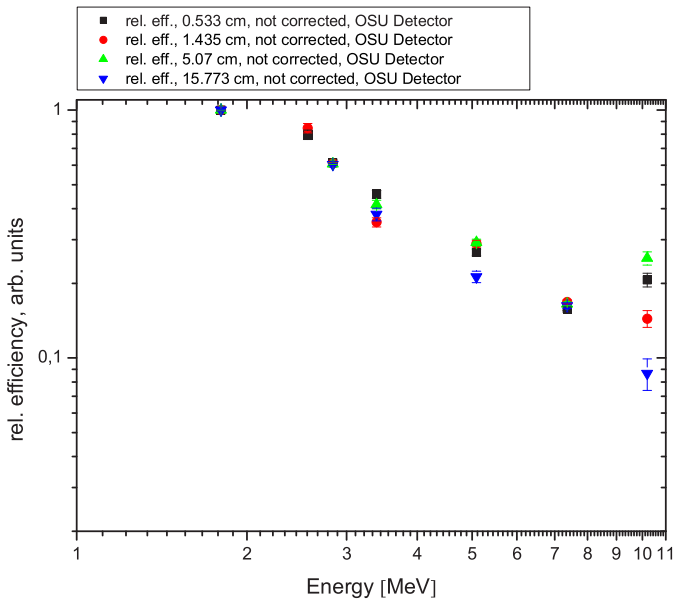

Figure 3.9: Relative efficiency of the OSU detector for different distances, no summing corrections.

Table 3.4: Calculated values of the relative efficiency for different distances and energies, OSU detector, no summing corrections, part I.

E_γ	$\epsilon^{uncorrected}_{0.533cm}$	$\Delta\epsilon^{uncorrected}_{0.533cm}$	$\epsilon^{uncorrected}_{1.435cm}$	$\Delta\epsilon^{uncorrected}_{1.435cm}$
1.799	1.0000	0.00606	1.0000	0.00628
2.56	0.7951	0.03449	0.8468	0.03689
2.838	0.6118	0.00420	0.6095	0.00434
3.389	0.4576	0.01648	0.3530	0.01500
5.089	0.2667	0.00840	0.2894	0.00907
7.36	0.1583	0.00273	0.1685	0.00292
10.198	0.2066	0.01294	0.1440	0.01117

Table 3.5: Calculated values of the relative efficiency for different distances and energies, OSU detector, no summing corrections, part II.

E_γ	$\epsilon^{uncorrected}_{5.07cm}$ 5,07	$\Delta\epsilon^{uncorrected}_{5.07cm}$	$\epsilon^{uncorrected}_{15.773cm}$ 15,773	$\Delta\epsilon^{uncorrected}_{15.773cm}$
1.799	1.0000	0.00647	1.0000	0.00911
2.56	–	–	–	–
2.838	0.6067	0.00447	0.6039	0.00627
3.389	0.4162	0.01680	0.3800	0.02258
5.089	0.2925	0.00940	0.2129	0.01129
7.36	0.1653	0.00298	0.1626	0.00416
10.198	0.2525	0.01522	0.0866	0.01251

The listed values follow the expected trend for the efficiency dependence on energy. For the determination of the absolute efficiency, the relative efficiency was fitted with the function:

$$f(x) = 10^{(P1 \times log(x) + P2)} \tag{3.10}$$

where P1 and P2 are the fit parameters. Two fit functions, one for a low energy region and one for a high energy region, have been calculated. The next step was the division of the absolute efficiency that has been determined with the radioactive sources by the calculated value of the fit function. This result is a scaling factor which allows for conversion of the relative efficiency into the absolute efficiency (see figures 3.10 and 3.11).

It is worth noting, that the calculated efficiency values are not corrected with summing corrections. Therefore they were not used to determine cross sections and other parameters.

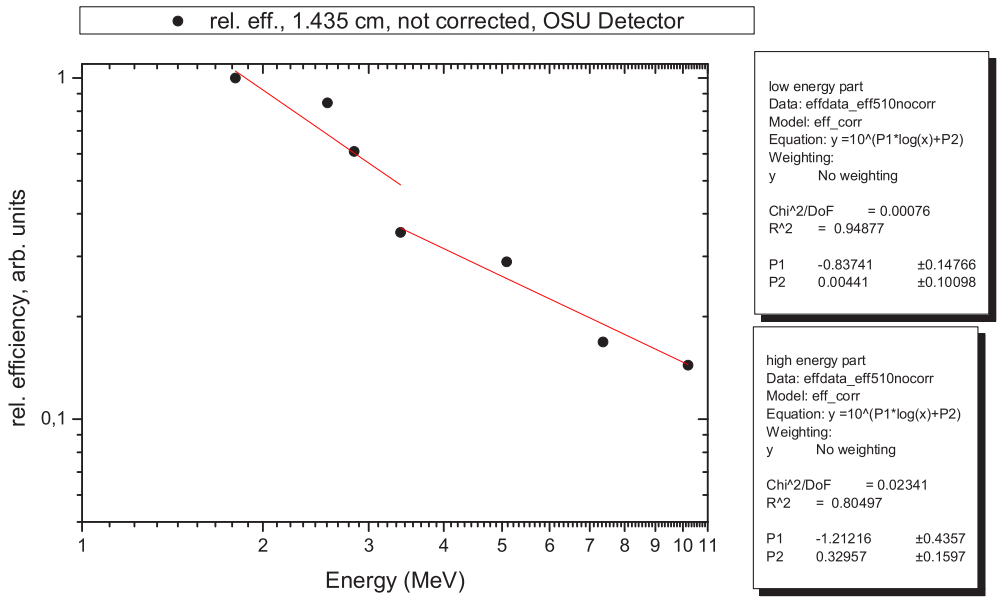

Figure 3.10: Example for the calculated fit functions, OSU detector, no summing corrections.

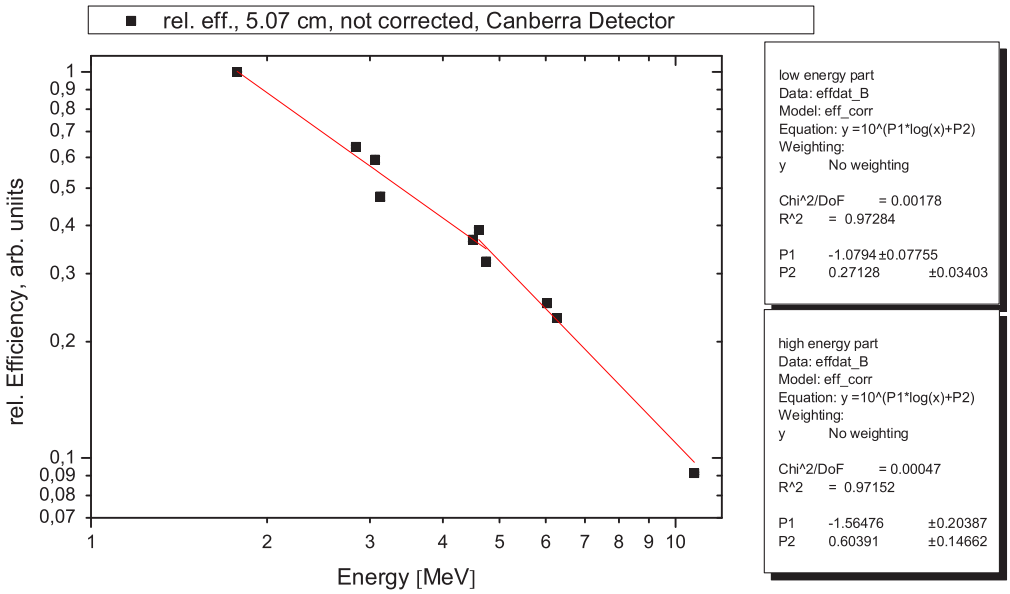

Figure 3.11: Example for the calculated fit functions, Canberra detector, no summing corrections.

3.2.2 Summing corrections

Detailed information about summing corrections are given in the books of Knoll [8] and Debertin [14].

A consideration of the summing effects occurring in these experiments, is given in this section.

Calculation of summing correction for $^{27}Al(p,\gamma)^{28}Si$

The summing corrections for the $^{27}Al(p,\gamma)^{28}Si$ reaction have been calculated. The first step was to calculate the total efficiency way calculated with the help of the programm *toteff* developed by Prof. Joachim Görres, which calculates the total efficiency of a Ge detector. Then, each correction factor has been calculated and multiplied with the event counts. The expression for the corrected efficiency is :

$$\epsilon_{rel}^{\text{corr}}(\Delta E_\gamma) = \frac{N_i}{(I/I_0)_{gesamt} \times BR \times N_{rel} \times (1 - c_i)} \tag{3.11}$$

where N_{rel} is the number of events for the transition, for which the efficiency will be determined relatively (see tables 3.6 and 3.7).

The detailed example calculations can be found in Appendix A.

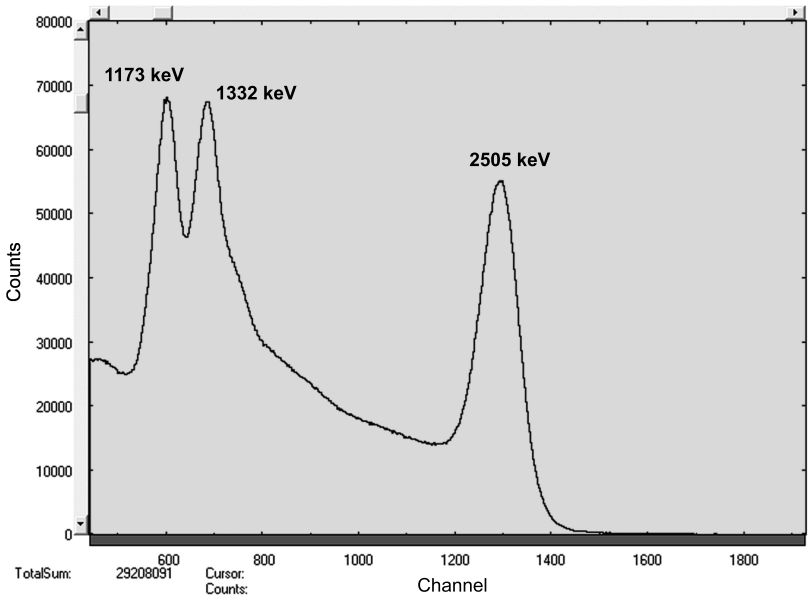

Figure 3.12: Illustration of summing in, based on a sum peak of a ^{60}Co spectrum.

Table 3.6: Example values for the correction factors and the resulting efficiency values, Canberra detector, $E_p = 992\,k$eV, distance of 5.07 cm.

i	E_γ	ϵ_{toteff}	c_i	ϵ_i^{corr}	$\Delta\epsilon_i^{corr}$
1	10764	0.0171	0.0209	0.0962	0.00060
2	7925	0.0167	0.0394	0.1069	0.00245
3	6266	0.0167	0.0407	0.2473	0.00533
6	4743	0.017	0.0521	0.3508	0.00314
7	4609	0.017	0.0225	0.4102	0.00523
8	3125	0.0182	0.0705	0.5271	0.01250
9	3063	0.0182	0.0215	0.6238	0.01161
25	6021	0.0167	0.0379	0.2693	0.00033
27	1523	0.0218	0.0577	1.1502	0.00094
33	4498	0.0171	0.0507	0.3991	0.00027
36	2839	0.0185	0.0462	0.6916	0.00034
37	1778	0.0209	0.0287	1.0000	0.00167

Table 3.7: Example values for the correction factors and the resulting efficiency values, OSU detector, $E_p = 406\,k\text{eV}$, distance of $5.07\,c\text{m}$.

i	E_γ	ϵ_{toteff}	c_i	ϵ_i^{corr}	$\Delta\epsilon_i^{corr}$
1	10198	0.0148	0.0181	0.1597	0.01558
2	7360	0.0145	0.0342	0.1752	0.00305
5	5089	0.0147	0.0335	0.3098	0.00963
6	3389	0.0156	0.0346	0.4413	0.01719
37	2838	0.0161	0.0335	0.4777	0.00431
38	1778	0.0181	0.0310	1.0000	0.00624

Comparison of the corrected and uncorrected detector efficiency

To clarify the effect of the summing corrections, the ratio of the uncorrected and corrected efficiencies have been calculated.

$$\epsilon_{ratio}(d) = \frac{\epsilon_i^{corr}(d)}{\epsilon_i^{nocorr}(d)} \tag{3.12}$$

The parameter d is the distance between the end of the target holder and the detector cap (see tables 3.8, 3.9 and 3.9). In figures 3.13 and 3.14 the uncorrected and corrected efficiencies are plotted.

In general the summing corrections and the efficiencies follow the expected trends. The determination of the absolute efficiencies followed the same procedure as for the uncorrected efficiencies (see section 3.2.1).

Table 3.8: Example values for the ratios between corrected and uncorrected efficiency, Canberra detector, $E_p = 992\,k\text{eV}$, distance of $5.07\,c\text{m}$.

i	E_γ	ϵ_i^{nocorr}	$\Delta\epsilon_i^{corr}$	ϵ_i^{corr}	$\Delta\epsilon_i^{corr}$	$\epsilon_{ratio}(5.07cm)$
1	10764	0.0914	0.00058	0.0962	0.00060	1.0525
2	7925	0.0996	0.00238	0.1069	0.00245	1.0728
3	6266	0.2302	0.00517	0.2473	0.00533	1.0742
6	4743	0.3227	0.00304	0.3508	0.00314	1.0871
7	4609	0.3891	0.00508	0.4102	0.00523	1.0542
8	3125	0.4755	0.01213	0.5271	0.01250	1.1087
9	3063	0.5924	0.01126	0.6238	0.01161	1.0531
25	6021	0.2514	0.00332	0.2693	0.00033	1.0711
27	1523	1.0517	0.00940	1.1502	0.00094	1.0936
33	4498	0.3677	0.00445	0.3991	0.00027	1.0855
36	2839	0.6401	0.00544	0.6916	0.00034	1.0804
37	1778	1.0000	0.00172	1.0000	0.00167	1.0000

Table 3.9: Listed are the efficiency ratios for different distances d and energies, $E_p = 406\,k\mathrm{eV}$, OSU detector.

i	E_γ	$\epsilon_{ratio}(0.533cm)$	$\epsilon_{ratio}(1.435cm)$	$\epsilon_{ratio}(5.07cm)$	$\epsilon_{ratio}(15.773cm)$
1	10198	0.6085	0.6187	0.6324	0.6360
2	7360	1.0743	1.0679	1.0598	1.0570
4	5099	1.0049	1.0220	1.0450	1.0539
5	5089	1.0697	1.0650	1.0590	1.0568
6	3389	1.0760	1.0691	1.0603	1.0570
7	2560	1.1251	1.1004	1.0700	1.0591
37	2838	0.7957	0.7921	0.7874	0.7857
38	1778	1.0000	1.0000	1.0000	1.0000

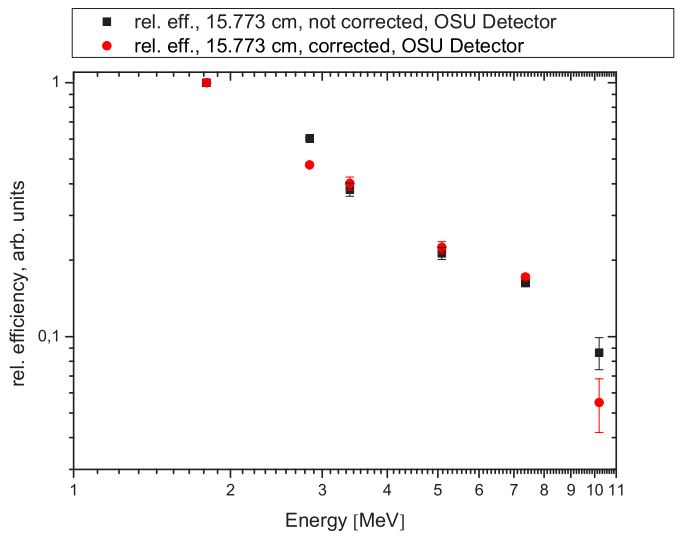

Figure 3.13: Corrected and uncorrected relative efficiency as a function of energy, OSU detector. Distance of 15.77 cm.

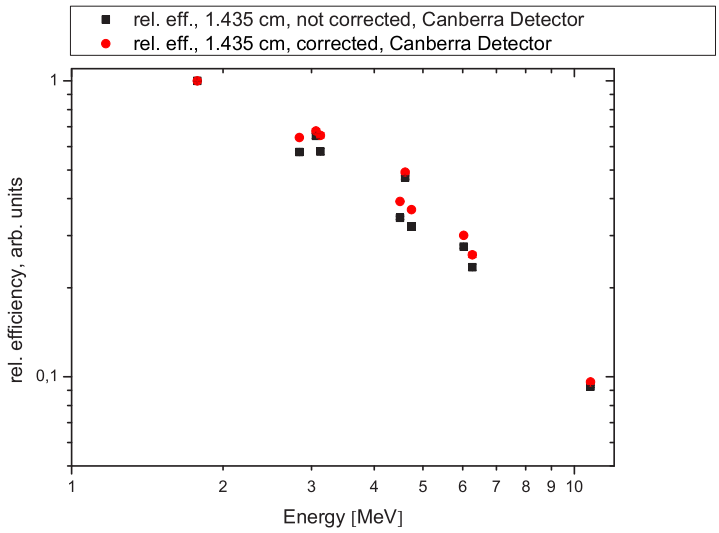

Figure 3.14: Corrected and not corrected relative efficiency as a function of energy, Canberra detector. Distance of 1.44 *c*m.

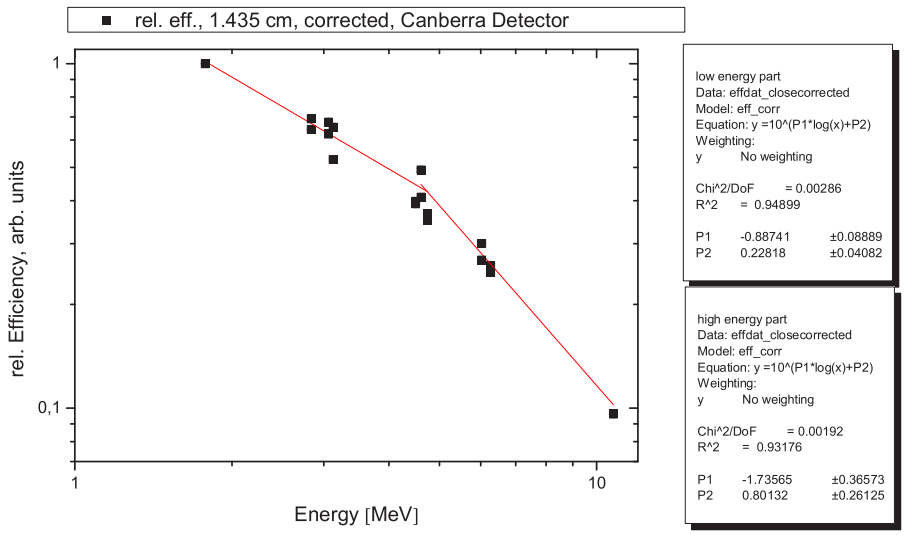

Figure 3.15: Example fit for the relative corrected efficiency as a function of energy. Canberra detector, distance of 1.44 *c*m.

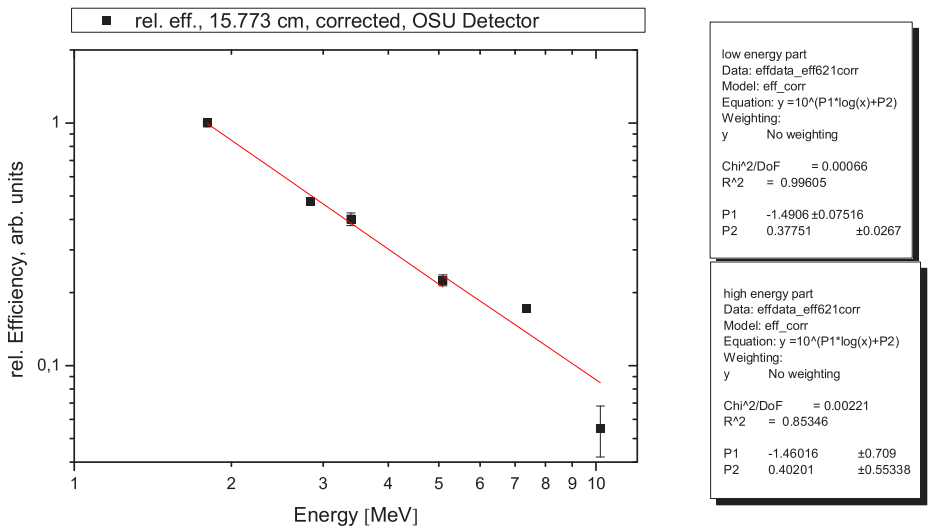

Figure 3.16: Example fit for the relative corrected efficiency as a function of energy. OSU detector, distance of 15.77 *cm*.

3.2.3 Determination of the detector efficiency for the NaI detectors.

Unfortunately, a determination of the efficiency for the NaI detectors could not be done in the detail as for the Ge detectors. The reason for that is the relative poor energy resolution, which made it impossible e.g. to identify single transitions of the $^{27}Al(p,\gamma)^{28}Si$ reaction. Only strong radioactive standard source measurement could be performed. Also the sum peak for ^{60}Co could be observed (see figure 3.12).

Table 3.10: Efficiency values for the NaI detectors and their sum signal

Source	E_γ	ϵ_{left}	$\Delta\epsilon_{left}$	ϵ_{right}	$\Delta\epsilon_{right}$	ϵ_{sum}	$\Delta\epsilon_{sum}$
^{60}Co	1173	0.06190	0.0015158	0.09513	0.0012330	0.06244	0.0015171
	1332	0.04473	0.0017721	0.06857	0.0014402	0.04232	0.0018300
^{137}Cs	662	0.13896	0.000004	0.15241	0.000004	0.29719	0.000004

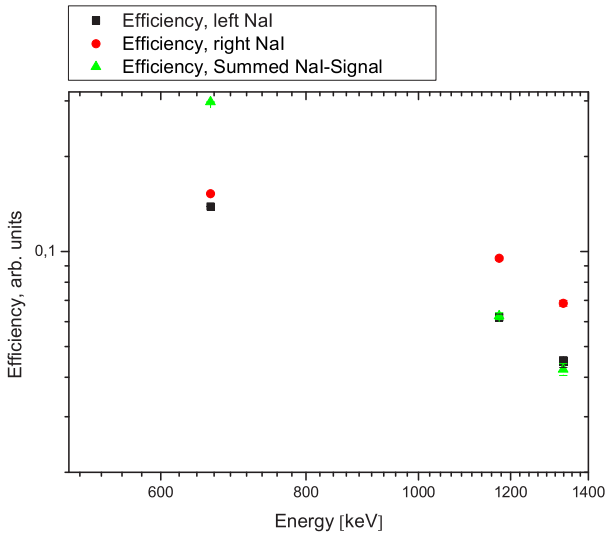

Figure 3.17: Plotted are the calculated efficiency values for the NaI detectors as a function of energy.

No fit functions have been calculated for the data shown in table 3.10 and in figure 3.17 because they are not neede for the cross section analysis.

3.2.4 Effects of Cosmic radiation suppression

To investigate the effects of Cosmic radiation suppression, the efficiency has been calculated for the coincidence spectra and was compared to the singles spectra.

$$\epsilon^i_{\text{ratio anticosmic}} = \frac{\epsilon^i_{\text{anticosmic}}}{\epsilon^i_{ungated}} \tag{3.13}$$

In particular, with the index i the different detector setups have been considered. No substantial effects on the efficiency could be observed (see tables 3.11, 3.12 and figure 3.18).

Table 3.11: Listed are the calculated efficiency ratios for different setups. The distances are 5.07 cm (Setup I), 1.44cm (Setup II) und 5.07 cm (Setup III).

E_γ	$\epsilon^1_{\text{ratio anticosmic}}$	$\epsilon^2_{\text{ratio anticosmic}}$	$\epsilon^3_{\text{ratio anticosmic}}$
7360	1.006	0.998	1.004
5099	1.075	0.966	1.002
5089	1.017	0.883	1.016
3389	0.677	0.938	0.969
2560	0.941	1.317	1.111
2838	0.951	1.000	1.021
1799	0.998	0.980	1.006

Table 3.12: For illustration purposes, the efficiency ratios are listed for setup III for several distances.

E_γ	$\epsilon^{0.533cm}_{\text{ratio anticosmic}}$	$\epsilon^{1.435cm}_{\text{ratio anticosmic}}$	$\epsilon^{5.07cm}_{\text{ratio anticosmic}}$	$\epsilon^{15.773cm}_{\text{ratio anticosmic}}$
7360	1.0092	0.9558	0.9470	0.9977
5099	0.9646	0.8389	0.8696	1.5791
5089	1.0000	0.9518	0.9518	1.1827
3389	0.9720	0.9487	0.9760	1.1727
2560	1.2258	0.9783	0.7981	0.4146
2838	0.9976	0.9983	1.0007	1.0014
1799	0.9976	0.9945	0.9969	0.9979

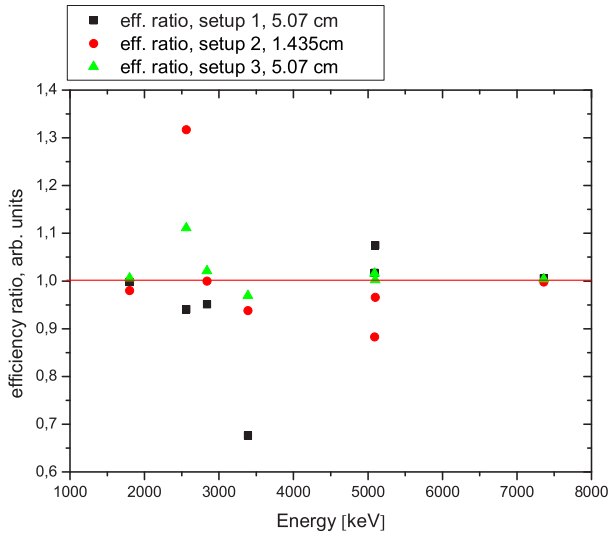

Figure 3.18: Plotted are the calculated efficiency values for specific transitions.

3.2.5 Effects of the Compton suppression on the detector efficiency

The main effect of the Compton suppression is the suppression of events resulting from cascade decays. Therefore, direct ground state transitions should be easier to identify than before.

Tables 3.13 and 3.14 show the effects for all setups, it can be seen that setup I is the optimal setup for Compton suppression.

Table 3.13: Efficiency ratios for the Compton suppression as a function of distance, setup III.

E_γ	$\epsilon^{0.533cm}_{\text{ratio anticompton}}$	$\epsilon^{1.435cm}_{\text{ratio anticompton}}$	$\epsilon^{5.07cm}_{\text{ratio anticompton}}$	$\epsilon^{15.773cm}_{\text{ratio anticompton}}$
10198	0.7439	0.7358	0.2069	n.b.
7360	0.4503	0.4494	0.4766	0.4721
5099	0.4980	0.3250	0.5031	0.3980
5089	0.4491	0.5980	0.4452	0.5673
3389	0.4440	0.4148	0.4815	0.7470
2560	0.1075	0.3666	0.2903	0.1429
2838	0.4334	0.4353	0.4541	0.4587
1799	0.4304	0.4353	0.4559	0.4646

Table 3.14: Listed are the calculated efficiency ratios for different setups. Distances are 5.07cm (Setup I), 1.44 cm (Setup II) and 5.07cm (Setup III).

E_γ	$\epsilon^{1}_{\text{ratio anticompton}}$	$\epsilon^{2}_{\text{ratio anticompton}}$	$\epsilon^{3}_{\text{ratio anticompton}}$
10198	n.b.	0.750	0.207
7360	0.0675	0.271	0.477
5099	n.b.	0.186	0.503
5089	n.b.	0.202	0.445
3389	n.b.	0.568	0.481
2560	n.b.	0.000	0.290
2838	0.0585	0.260	0.454
1799	0.0716	0.279	0.456

The $^{27}Al(p,\gamma)^{28}Si$ resonances previously investigated did not include a direct ground state transitions. In the following the Compton suppression discussion including the 505 keV resonance is included which involves a ground state transition. In particular this transition can give detailed information about the loss of physically interesting events. For example, such a loss can be caused by simultaneous coincident events. Looking at the singles spectrum and the coincidence spectrum, a perfect suppression and timing would not effect the number of events for the ground state transition. Only a reduction of the background should be observable.

In an energy range of $E_p = 500\,k\text{eV} - 510\,k\text{eV}$ two resonances at $505\,k\text{eV}$ and $507\ k\text{eV}$ exist for the reaction $^{27}Al(p,\gamma)^{28}Si$. The populated resonance states decay to the ground state with 55% and 16%, for $E_r = 505\,k\text{eV}$ and $E_r = 507\,k\text{eV}$, respectively (see table 3.15). The current analysis is included because right now not possible to observe both resonances separately.

Table 3.15: For the $E_p = 505\,k$eV and $E_p = 507\,k$eV resonance the ground state transitions and their branching ratios are listed; from Meyer et al. [12].

E_p	E_R	$BR_{R\to 0}$ (%)	$BR_{R\to 1778}$ (%)
505	12072	55	14
507	12074	16	44

It should to be noted that the relative efficiency for the ground state transitions should increase, since the transition from the first excited state to the ground state is suppressed (see table 3.16) .

Table 3.16: Efficiency ratios for the 505 keV resonance for different distances and setups. The indices of the distances indicated whether a singles or coincidence spectrum.

Abstand (cm)	$\epsilon_{\text{ratio anticompton}}$
$0.53_{singles}$	0.0780
$0.53_{coincidence}$	0.1618
$1.44_{singles}$	0.0929
$1.44_{coincidence}$	0.1972
$5.07_{singles}$	0.0766
$5.07_{coincidence}$	0.1213
$15.77_{singles}$	0.1002
$15.77_{coincidence}$	0.1954

From table 3.16, it can be seen that the relative efficiency increases up to a factor of 2. The results for the ground state transitions are only from setup III.
For the different setups, it is clearly observable, that the Compton suppression leads definitively to an improvement in terms of background reduction and detector efficiency.
To answer the question which setup would be the best to investigate direct capture, a detailed analysis is needed, which would go beyond the scope of this report.
An aspect which has not been taken in to consideration, was for example angular distribution effects, between setup I and setup III. This effects directly the calculation and determination of resonance strengths, cross section etc.
One continued problem is that gain shifts of the NaI detectors could not be observed during the real experiments.
Also, a detailed analysis with computer simulations would give a more detailed picture of the advantages and disadvantages of the different setups.

Chapter 4

Results for the reaction $^{20}Ne(p,\gamma)^{21}Na$

As we noted in chapter 2, there existed experimental problems that did not allow for the extraction of useful data from the first experiment. However, during the 2nd experiment Setup III was used to investigate the reaction $^{20}Ne(p,\gamma)^{21}Na$, and a high counting rate was achieved.

4.1 Resonance strength of the $E_p = 1169\,k\text{eV}$ resonance

The resonance strength $\omega\gamma$ is defined by the following equations :

$$\omega\gamma = \frac{(2J+1)}{(2s+1)(2j+1)}\frac{\Gamma_i\Gamma_l}{\Gamma} \tag{4.1}$$

For thick targets, the resonance strength can be calculated via :

$$\omega\gamma = \frac{2}{\lambda^2}\frac{M}{m+M}\frac{dE}{dx}Y_\infty \tag{4.2}$$

To determine the target thickness, the resonance $E_p = 1169\,k\text{eV}$ was measured. To determine changes in target profile and thickness, the resonance was measured several times during the experiment. The target thickness can be determined from the Full Width Half Maximum of the excitation curve of the resonance.
A target thickness of $\Delta E_t \approx 25\,k\text{eV}$ was determined. Therefore, in the following calculations equation 4.2 will be used.
The yield has been determined with following equation :

$$Y_\infty = \frac{N_\gamma}{N_p \times I/I_0 \times BR \times W(\theta) \times \epsilon} \tag{4.3}$$

with

$$N_p = \frac{Q \times 10^{-8}}{e} \tag{4.4}$$

The factor 10^{-8} is based on the scaling factor of the used Charge Integrators.
The de-Broglie wave length can be calculated by :

$$\lambda = \frac{m+M}{M}\frac{\hbar}{\sqrt{2mE_l}} \tag{4.5}$$

which in our case is :

$$\begin{aligned}\lambda &= \frac{m_p + M_{^{20}Ne}}{M_{^{20}Ne}}\frac{\hbar}{\sqrt{2m_pE_p}} \\ &= \frac{21}{20}\frac{h}{\sqrt{2m_pE_p}}\end{aligned} \tag{4.6}$$

The determination of dE/dx was performed with the simulation program SRIM[1]. The program generated a table for the energy loss as a function of energy. Since the energy steps in the generated table were not available in the necessary 1 keV steps, the software OriginPro was used to interpolate the data points. The unit eV/($10^{15} atoms/cm^2$) was used, to allow a easier handling afterwards (see figure 4.1).

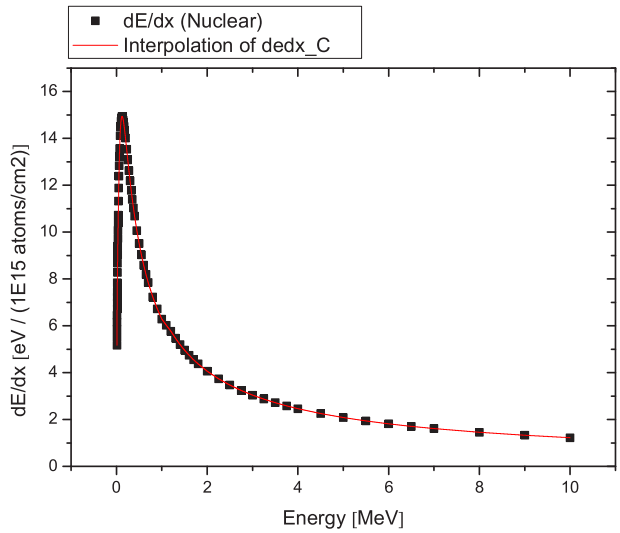

Figure 4.1: Plot of the calculated values for the energy loss. Also plotted is the interpolation curve, generated by OriginPro.

As an example, the calculation for the resonance strength for one experimental run is shown. The energy of the proton for the example is $E_p = 1185.21\ keV$.

The de-Broglie wave length is then :

[1]SRIM stands for *The Stopping and Range of Ions in Matter*, developed by J.Ziegler, www.srim.org.

$$\begin{aligned}\lambda &= \frac{m_p + M_{^{20}Ne}}{M_{^{20}Ne}} \frac{h}{\sqrt{2m_pE_p}} \\ &= \frac{21}{20} \frac{h}{\sqrt{2m_pE_p}} \\ &= 1.05 \times \frac{4.1357 \times 10^{-15}\,\mathrm{eV\,s}}{\sqrt{2 \times 938.271 \times 10^6\,\mathrm{eV}/(3 \times 10^8\,\mathrm{m/s})^2 \times 1185.21 \times 10^3\,\mathrm{eV}}} \\ &= 2.76236 \times 10^{-12}\,cm\end{aligned} \tag{4.7}$$

and its square :

$$\lambda^2 = 7.63061 \times 10^{-24}\,cm^2 \tag{4.8}$$

From the interpolation curve the value for the energy loss is:

$$\frac{dE}{dx}_{(1185.21\,k\mathrm{eV})} = 5.807 \times 10^{-15}\,\mathrm{eV}\,cm^2 \tag{4.9}$$

The yield is then :

$$\begin{aligned}Y_\infty &= \frac{5310 \times 1.44}{3.12072 \times 10^{16} \times 0.9991 \times 0.919 \times 3.50 \times 10^{-4}} \\ &= (7.628 \pm 0,11) \times 10^{-10}\end{aligned} \tag{4.10}$$

The resonance strength is then :

$$\begin{aligned}\omega\gamma &= \frac{2}{\lambda^2} \frac{M}{m+M} \frac{dE}{dx} Y_\infty \\ &= \frac{2 \times 5.807 \times 10^{-15}\,\mathrm{eV}\,cm^2}{7.63061 \times 10^{-24}\,cm^2} \times \frac{20}{21} \times 7.628 \times 10^{-10} \\ &= 1.11 \pm 0.02\,\mathrm{eV}\end{aligned} \tag{4.11}$$

After analyzing all useful measurements and calculating the average, the resulting resonance strength was found to be :

$$\omega\gamma = 1.12 \pm 0.02\,\mathrm{eV} \tag{4.12}$$

A comparison with the values of Tanner et al. [5] and Stech [7] (see table 4.1) shows an agreement.

Table 4.1: Comparison of the in this work achieved results and previous results for the resonance strength $\omega\gamma$. The value in the last column is a weighted average by Stech [7].

Reference	$\omega\gamma$(eV)
this work	1.12 ± 0.02
[7]	1.17 ± 0.06
[5]	1.13 ± 0.07
[7] weighted average	1.06 ± 0.07

4.2 Cross section for non-resonant energies

The cross section for direct capture reactions can be calculated using the following:

$$\sigma_{DC} = \frac{1}{2}\lambda^2 \frac{m+M}{M} \frac{\omega\gamma}{\Delta} (\frac{Y_{DC}}{Y_R}) \tag{4.13}$$

$$\frac{Y_{DC}}{Y_R} = \frac{N_{DC}}{N_R} \frac{\epsilon_R}{\epsilon_{DC}} \frac{\Omega_R}{\Omega_{DC}} \frac{W_R(\theta)}{W_{DC}(\theta)} \tag{4.14}$$

It also has to be distinguished for which component of the direct capture reaction the cross section is calculated. Different resonance strengths from previous works and an average for the resonance strengths has been used.

For each transition, the energies of the expected γ-lines have been calculated and are listed in table 4.2.

Table 4.2: Energies of the expected γ-lines for the transitions of the $^{20}Ne(p,\gamma)^{21}Na$ reaction. The values for $2425 \rightarrow 0$ and $332 \rightarrow 0$ are not listed. Values are in keV.

E_p	E_{DC}	$E_\gamma(DC \rightarrow 2425)$	$E_\gamma(DC \rightarrow 332)$	$E_\gamma(DC \rightarrow 0)$
600	3003.43	578.43	2671.43	3003.43
750	3146.29	721.29	2814.29	3146.29
850	3241.52	816.52	2909.52	3241.52
925	3312.95	887.95	2980.95	3312.95
925	3312.95	887.95	2980.95	3312.95
1050	3432.00	1007.00	3100.00	3432.00
1099.99	3479.61	1054.61	3147.61	3479.61
1100	3479.62	1054.62	3147.62	3479.62
1160.04	3536.80	1111.80	3204.80	3536.80

The experimental data only allowed a determination of events for the $2425 \rightarrow 0$ transition (see section **??**).

Figure 1.3 shows that the transitions $DC \rightarrow 2425$ feeds directly the 2425 keV state. Therefore, the cross section of the $DC \rightarrow 2425$ component could be determined with the transition $2425 \rightarrow 0$.

The results are listed in table 4.3 and plotted in figure 4.2.

Table 4.3: Listed are the calculated cross sections for the $DC \rightarrow 2425$ as a function of energy. The value for $\omega\gamma$ calculated in this work has been used.

E_p (keV)	$\sigma_{DC\rightarrow 2425}$ (μb)
600	0.119 ± 0.003
750	0.151 ± 0.004
850	0.257 ± 0.009
925	0.357 ± 0.015
925	0.384 ± 0.017
925 (average)	0.371 ± 0.016
1050	0.580 ± 0.033
1100	0.726 ± 0.046
1100	0.600 ± 0.035
1100 (average)	0.663 ± 0.041
1160	2.280 ± 0.261

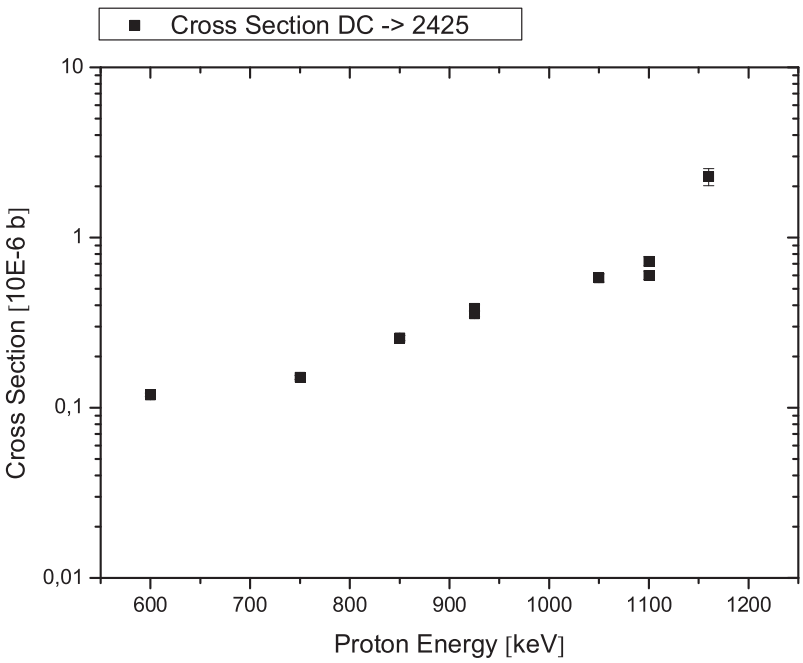

Figure 4.2: Plotted are the calculated cross sections as a function of energy.

Table 4.5: Listed are the calculated cross sections using the weighted $\omega\gamma$ average in reference [7] and our $\omega\gamma$.

E_p	$\omega\gamma = 1.06 \pm 0.07$	$\omega\gamma = 1.09 \pm 0.04$
	weighted average from [7]	average from this work
600	0.113 ± 0.002	0.116 ± 0.003
750	0.143 ± 0.004	0.147 ± 0.004
850	0.243 ± 0.009	0.250 ± 0.009
925	0.338 ± 0.014	0.348 ± 0.015
925	0.364 ± 0.016	0.374 ± 0.017
925 (average)	0.351 ± 0.015	0.361 ± 0.016
1050	0.549 ± 0.031	0.565 ± 0.032
1100	0.687 ± 0.044	0.707 ± 0.045
1100	0.568 ± 0.033	0.584 ± 0.034
1100 (average)	0.628 ± 0.038	0.645 ± 0.040
1160	2.158 ± 0.247	2.219 ± 0.254

4.2.1 Comparison with previous results

An important aspect of the comparison with previous results is the fact that different resonance strengths have been used. This was taken into account when calculating the cross sections with the different resonance strengths (see tables 4.4 and 4.5, as well as figure 4.3).

Table 4.4: Listed are the calculated values for the cross section using the resonance strengths listed the in references [5], [6] and [7].

E_p	$\omega\gamma = 1.12 \pm 0.02$	$\omega\gamma = 1.13 \pm 0.06$	$\omega\gamma = 1.17 \pm 0.06$
	this work	Tanner et al. [5]	Stech [7]
600	0.119 ± 0.003	0.120 ± 0.003	0.124 ± 0.003
750	0.151 ± 0.004	0.153 ± 0.004	0.158 ± 0.005
850	0.257 ± 0.009	0.259 ± 0.010	0.268 ± 0.012
925	0.357 ± 0.015	0.360 ± 0.017	0.373 ± 0.020
925	0.384 ± 0.017	0.388 ± 0.019	0.401 ± 0.023
925 (average)	0.371 ± 0.016	0.374 ± 0.018	0.387 ± 0.021
1050	0.580 ± 0.033	0.585 ± 0.037	0.606 ± 0.043
1100	0.726 ± 0.046	0.733 ± 0.052	0.759 ± 0.061
1100	0.600 ± 0.035	0.605 ± 0.039	0.627 ± 0.046
1100 (average)	0.663 ± 0.041	0.669 ± 0.046	0.693 ± 0.054
1160	2.280 ± 0.261	2.301 ± 0.295	2.382 ± 0.346

Based on the fact that the results lay relatively close, the results match the expectations (see table 4.4 and 4.5).

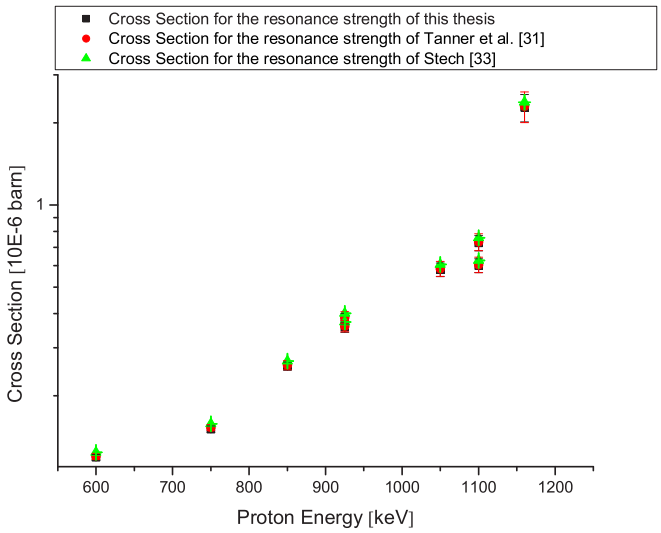

Figure 4.3: Plotted are the calculated cross sections as a function of proton energy for different resonance strengths.

The experimental results from Stech [7] and Rolfs [6] have been taken and have been plotted in figure 4.4 using our results for the $DC \rightarrow 2425$ component. Figure 4.4 shows that the trend of the experimental results are in good agreement and that the absolute values have a fair agreement.

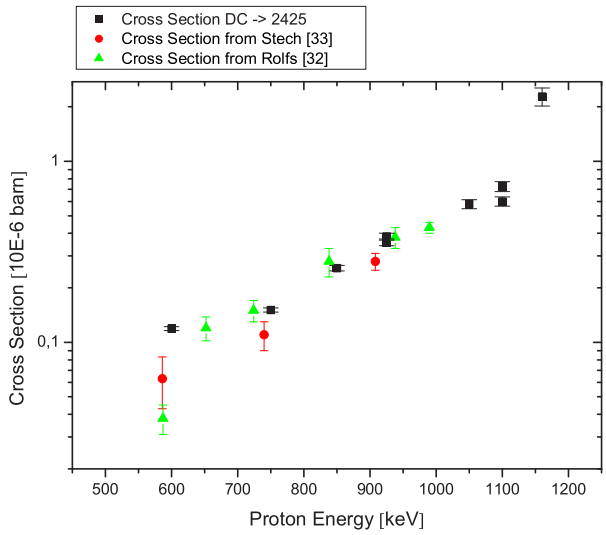

Figure 4.4: Illustrated are the calculated cross sections from this work and the work of Stech [7] and Rolfs [6].

Chapter 5

Conclusions and Outlook

The reaction $^{20}Ne(p,\gamma)^{21}Na$ has been studied with two experiments at the Nuclear Structure Laboratory at the University of Notre Dame.
Several experimental problems arose during the experiments that either caused delays or worsened the quality of the data. Some of these problems were machine related, whereas others were caused by previously unknown factors. However, despite these issues, the resonance strength was found to be $1.12 \pm 0.02\,\mathrm{eV}$, which is in agreement with Tanner [5] and Stech [7]. Additionally, invaluable experience was gained that can be used in future experiments to increase the likelihood of success. This included a setup with optimal Cosmic and Compton radiation suppression using the available detectors.
In the future there are several topics that could be addressed to further improve the outcome. For instance the method of calculating the detector efficiency should be reconsidered, possibly using the matrix method of Semkow et al. [15], would give a better insight into the efficiency properties of each setup. Additionally, computer simulations with codes like GEANT4 would enhance the knowledge of each detector setup and might indicate the optimal mechanical properties. In general a series of experiments using solid state targets and a gas target system should be performed to resolve any inconsistencies in target effects. When the cross section and all of its components are determined a calculation of the astrophysical S-Factor and the implementation of the results into reaction networks should be performed. Only then, a statement about the effects on the Astrophysics would be possible.

Appendix A

Appendix

A.1 Calculation of summing corrections

Summing corrections for $^{27}Al\,(p,\gamma)^{28}\,Si$ at $E_p = 992\,k\mathrm{eV}$

Given in the following are the summing corrections for $^{27}Al\,(p,\gamma)^{28}\,Si$ at $E_p = 992\,k\mathrm{eV}$. The base for the calculations is figure A.1.
The bold arrows are the transitions, for which the efficiency was calculated. ϵ_i is the efficiency for the specific transition i. I_i is the branching ratio, while N_i is the normalizing factor for the specific transition.
For illustration the calculations for transition 33 ($6276\,k\mathrm{eV} \rightarrow 1778\,k\mathrm{eV}$, Peak at $E_\gamma = 4498\,k\mathrm{eV}$) are shown in detail.

Transition 1, $12542\,k\mathrm{eV} \rightarrow 1778\,k\mathrm{eV}$, Peak at $E_\gamma = 10764\,k\mathrm{eV}$

$$\begin{aligned} c_1 &= \left(\frac{I_1 I_{37}}{N_1}\right)\epsilon_{37} \\ &= \epsilon_{37} \end{aligned}$$

Transition 2, $12542\,k\mathrm{eV} \rightarrow 4618\,k\mathrm{eV}$, Peak at $E_\gamma = 7924\,k\mathrm{eV}$

$$\begin{aligned} c_2 &= \left(\frac{I_2 I_{36} I_{37}}{N_2}\right)(\epsilon_{36} + \epsilon_{37}) \\ &= \epsilon_{36} + \epsilon_{37} \end{aligned}$$

Transition 3, $12542\,k\mathrm{eV} \rightarrow 6276\,k\mathrm{eV}$, Peak at $E_\gamma = 6266\,k\mathrm{eV}$

$$\begin{aligned} c_3 &= \left(\frac{I_3 I_{33} I_{37}}{N_3}\right)(\epsilon_{33} + \epsilon_{37}) + \left(\frac{I_3 I_{34} I_{36} I_{37}}{N_3}\right)(\epsilon_{34} + \epsilon_{36} + \epsilon_{37}) \\ &= 0.882\,(\epsilon_{33} + \epsilon_{37}) + 0.118\,(\epsilon_{34} + \epsilon_{36} + \epsilon_{37}) \end{aligned}$$

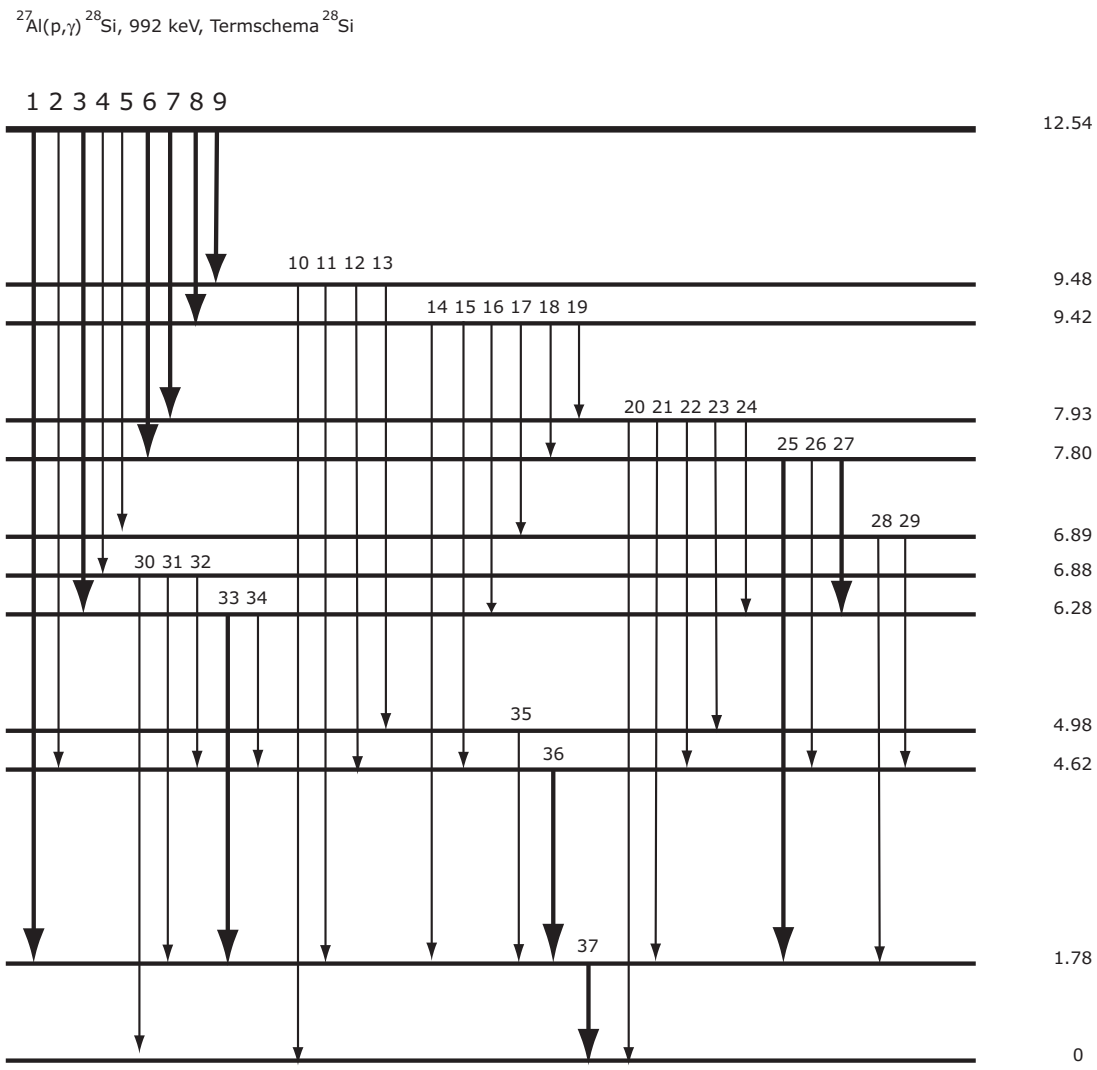

Figure A.1: Simplified decay scheme of ^{28}Si at $E_p = 992\,k\text{eV}$.

Transition 6, $12542\,k\text{eV} \rightarrow 7799\,k\text{eV}$, Peak at $E_\gamma = 4743\,k\text{eV}$

$$
\begin{aligned}
c_6 &= \left(\frac{I_6 I_{25} I_{37}}{N_6}\right)(\epsilon_{25}+\epsilon_{37}) + \left(\frac{I_6 I_{26} I_{36} I_{37}}{N_6}\right)(\epsilon_{25}+\epsilon_{36}+\epsilon_{37}) \\
&+ \left(\frac{I_6 I_{27} I_{33} I_{37}}{N_6}\right)(\epsilon_{27}+\epsilon_{33}+\epsilon_{37}) + \left(\frac{I_6 I_{27} I_{34} I_{36} I_{37}}{N_6}\right)(\epsilon_{27}+\epsilon_{34}+\epsilon_{36}+\epsilon_{37}) \\
&= 0.65\,(\epsilon_{25}+\epsilon_{37}) + 0.0132\,(\epsilon_{26}+\epsilon_{36}+\epsilon_{37}) + 0.2795\,(\epsilon_{27}+\epsilon_{33}+\epsilon_{37}) + 0.0401\,(\epsilon_{27}+\epsilon_{34}+\epsilon_{36}+\epsilon_{37})
\end{aligned}
$$

Transition 7, 12542 keV $\rightarrow$ 7933 keV, Peak at $E_\gamma = 4609\,k$eV

$$
\begin{aligned}
c_7 &= \left(\frac{I_7 I_{20}}{N_7}\right)\epsilon_{20} + \left(\frac{I_7 I_{21} I_{37}}{N_7}\right)(\epsilon_{21}+\epsilon_{37}) \\
&+ \left(\frac{I_7 I_{22} I_{36} I_{37}}{N_7}\right)(\epsilon_{22}+\epsilon_{36}+\epsilon_{37}) + \left(\frac{I_7 I_{23} I_{35} I_{37}}{N_7}\right)(\epsilon_{23}+\epsilon_{35}+\epsilon_{37}) \\
&+ \left(\frac{I_7 I_{24} I_{33} I_{37}}{N_7}\right)(\epsilon_{24}+\epsilon_{33}+\epsilon_{37}) + \left(\frac{I_7 I_{24} I_{34} I_{36} I_{37}}{N_7}\right)(\epsilon_{24}+\epsilon_{34}+\epsilon_{36}+\epsilon_{37}) \\
&= 0.834\epsilon_{20} + 0.055\,(\epsilon_{21}+\epsilon_{37}) + 0.047\,(\epsilon_{22}+\epsilon_{36}+\epsilon_{37}) \\
&+ 0.04\,(\epsilon_{23}+\epsilon_{35}+\epsilon_{37}) + 0.0211\,(\epsilon_{24}+\epsilon_{33}+\epsilon_{37}) + 0.0028\,(\epsilon_{24}+\epsilon_{34}+\epsilon_{36}+\epsilon_{37})
\end{aligned}
$$

Transition 8, 12542 keV $\rightarrow$ 9417 keV, Peak at $E_\gamma = 3125\,k$eV

$$
\begin{aligned}
c_8 &= \left(\frac{I_8 I_{14} I_{37}}{N_8}\right)(\epsilon_{14}+\epsilon_{37}) + \left(\frac{I_8 I_{15} I_{36} I_{37}}{N_8}\right)(\epsilon_{15}+\epsilon_{36}+\epsilon_{37}) \\
&+ \left(\frac{I_8 I_{16} I_{33} I_{37}}{N_8}\right)(\epsilon_{16}+\epsilon_{33}+\epsilon_{37}) + \left(\frac{I_8 I_{16} I_{34} I_{36} I_{37}}{N_8}\right)(\epsilon_{16}+\epsilon_{34}+\epsilon_{36}+\epsilon_{37}) \\
&+ \left(\frac{I_8 I_{17} I_{28} I_{37}}{N_8}\right)(\epsilon_{17}+\epsilon_{28}+\epsilon_{37}) + \left(\frac{I_8 I_{17} I_{29} I_{36} I_{37}}{N_8}\right)(\epsilon_{17}+\epsilon_{29}+\epsilon_{36}+\epsilon_{37}) \\
&+ \left(\frac{I_8 I_{18} I_{25} I_{37}}{N_8}\right)(\epsilon_{18}+\epsilon_{25}+\epsilon_{37}) + \left(\frac{I_8 I_{18} I_{26} I_{36} I_{37}}{N_8}\right)(\epsilon_{18}+\epsilon_{26}+\epsilon_{36}+\epsilon_{37}) \\
&+ \left(\frac{I_8 I_{18} I_{27} I_{33} I_{37}}{N_8}\right)(\epsilon_{18}+\epsilon_{27}+\epsilon_{33}+\epsilon_{37}) + \left(\frac{I_8 I_{18} I_{27} I_{34} I_{36} I_{37}}{N_8}\right)(\epsilon_{18}+\epsilon_{27}+\epsilon_{34}+\epsilon_{36}+\epsilon_{37}) \\
&+ \left(\frac{I_8 I_{19} I_{20}}{N_8}\right)(\epsilon_{19}+\epsilon_{20}) + \left(\frac{I_8 I_{19} I_{21} I_{37}}{N_8}\right)(\epsilon_{19}+\epsilon_{21}+\epsilon_{37}) + \left(\frac{I_8 I_{19} I_{22} I_{36} I_{37}}{N_8}\right)(\epsilon_{19}+\epsilon_{22}+\epsilon_{36}+\epsilon_{37}) \\
&+ \left(\frac{I_8 I_{19} I_{23} I_{35} I_{37}}{N_8}\right)(\epsilon_{19}+\epsilon_{23}+\epsilon_{35}+\epsilon_{37}) + \left(\frac{I_8 I_{19} I_{24} I_{33} I_{37}}{N_8}\right)(\epsilon_{19}+\epsilon_{24}+\epsilon_{33}+\epsilon_{37}) \\
&+ \left(\frac{I_8 I_{19} I_{24} I_{34} I_{36} I_{37}}{N_8}\right)(\epsilon_{19}+\epsilon_{24}+\epsilon_{34}+\epsilon_{36}+\epsilon_{37}) \\
&= 0.331\,(\epsilon_{14}+\epsilon_{37}) + 0.361\,(\epsilon_{15}+\epsilon_{36}+\epsilon_{37}) + 0.0273\,(\epsilon_{16}+\epsilon_{33}+\epsilon_{37}) \\
&+ 0.0037\,(\epsilon_{16}+\epsilon_{34}+\epsilon_{36}+\epsilon_{37}) + 0.1846\,(\epsilon_{17}+\epsilon_{28}+\epsilon_{37}) \\
&+ 0.0024\,(\epsilon_{17}+\epsilon_{29}+\epsilon_{36}+\epsilon_{37}) + 0.0364\,(\epsilon_{18}+\epsilon_{25}+\epsilon_{37}) \\
&+ 0.0007\,(\epsilon_{18}+\epsilon_{26}+\epsilon_{36}+\epsilon_{37}) + 0.0168\,(\epsilon_{18}+\epsilon_{27}+\epsilon_{33}+\epsilon_{37}) \\
&+ 0.0022\,(\epsilon_{18}+\epsilon_{27}+\epsilon_{34}+\epsilon_{36}+\epsilon_{37}) + 0.0125\,(\epsilon_{19}+\epsilon_{20}) \\
&+ 0.0008\,(\epsilon_{19}+\epsilon_{21}+\epsilon_{37}) + 0.0007\,(\epsilon_{19}+\epsilon_{22}+\epsilon_{36}+\epsilon_{37}) \\
&+ 0.0006\,(\epsilon_{19}+\epsilon_{23}+\epsilon_{35}+\epsilon_{37}) + 0.0003\,(\epsilon_{19}+\epsilon_{24}+\epsilon_{33}+\epsilon_{37}) \\
&+ 0.0004\,(\epsilon_{19}+\epsilon_{24}+\epsilon_{34}+\epsilon_{36}+\epsilon_{37})
\end{aligned}
$$

Transition 9, 12542 keV $\rightarrow$ 9479 keV, Peak at $E_\gamma = 3063\,k$eV

$$
\begin{aligned}
c_9 &= \left(\frac{I_9 I_{10}}{N_9}\right)\epsilon_{10} + \left(\frac{I_9 I_{11} I_{37}}{N_9}\right)(\epsilon_{11}+\epsilon_{37}) \\
&+ \left(\frac{I_9 I_{12} I_{36} I_{37}}{N_9}\right)(\epsilon_{12}+\epsilon_{36}+\epsilon_{37}) + \left(\frac{I_9 I_{13} I_{35} I_{37}}{N_9}\right)(\epsilon_{13}+\epsilon_{35}+\epsilon_{37}) \\
&= 0.85\epsilon_{10} + 0.0258\,(\epsilon_{11}+\epsilon_{37}) + 0.064\,(\epsilon_{12}+\epsilon_{36}+\epsilon_{37}) + 0.045\,(\epsilon_{13}+\epsilon_{35}+\epsilon_{37})
\end{aligned}
$$

Transition 25, 7799 keV $\rightarrow$ 1788 keV, Peak at $E_\gamma = 6011\,k\text{eV}$

$$\begin{aligned} c_{25} &= \left(\frac{I_{25}I_6I_{37}}{N_{25}}\right)(\epsilon_6 + \epsilon_{37}) \\ &= (\epsilon_6 + \epsilon_{37}) \end{aligned}$$

Transition 27, 7799 keV $\rightarrow$ 6276 keV, Peak at $E_\gamma = 1523\,k\text{eV}$

$$\begin{aligned} N_{27} &= I_6I_{33}I_{37} + I_6I_{34}I_{36}I_{37} + I_8I_{18}I_{33}I_{37} + I_8I_{18}I_{34}I_{36}I_{37} \\ &= 0.0975 \end{aligned}$$

Inserting the branching ratios into the above relation gives :

$$\begin{aligned} c_{27} &= \left(\frac{I_{27}I_6I_{33}I_{37}}{N_{27}}\right)(\epsilon_6 + \epsilon_{33} + \epsilon_{37}) + \left(\frac{I_{27}I_6I_{34}I_{36}I_{37}}{N_{27}}\right)(\epsilon_6 + \epsilon_{34} + \epsilon_{36} + \epsilon_{37}) \\ &+ \left(\frac{I_{27}I_8I_{33}I_{37}}{N_{27}}\right)(\epsilon_8 + \epsilon_{33} + \epsilon_{37}) + \left(\frac{I_{27}I_8I_{18}I_{34}I_{36}I_{37}}{N_{27}}\right)(\epsilon_8 + \epsilon_{18} + \epsilon_{34} + \epsilon_{36} + \epsilon_{37}) \\ &= 0.8774\,(\epsilon_6 + \epsilon_{33} + \epsilon_{37}) + 0.1174\,(\epsilon_6 + \epsilon_{34} + \epsilon_{36} + \epsilon_{37}) \\ &+ 0.0046\,(\epsilon_8 + \epsilon_{33} + \epsilon_{37}) + 0.0006\,(\epsilon_8 + \epsilon_{18} + \epsilon_{34} + \epsilon_{36} + \epsilon_{37}) \end{aligned}$$

Transition 33, 6276 keV $\rightarrow$ 1778 keV, Peak at $E_\gamma = 4498\,k\text{eV}$

$$\begin{aligned} N_{33} &= I_3 + I_6I_{27} + I_7I_{24} + I_8\,(I_{16} + I_{18}I_{27} + I_{19}I_{24}) \\ &= 0.0584 \end{aligned}$$

$$\begin{aligned} c_{33} &= \left(\frac{I_{33}I_3I_{37}}{N_{33}}\right)(\epsilon_3 + \epsilon_{37}) + \left(\frac{I_{33}I_6I_{27}I_{37}}{N_{33}}\right)(\epsilon_6 + \epsilon_{27} + \epsilon_{37}) \\ &+ \left(\frac{I_{33}I_7I_{24}I_{37}}{N_{33}}\right)(\epsilon_7 + \epsilon_{34} + \epsilon_{37}) + \left(\frac{I_{33}I_8I_{16}I_{37}}{N_{33}}\right)(\epsilon_8 + \epsilon_{16} + \epsilon_{37}) \\ &+ \left(\frac{I_{33}I_8I_{18}I_{27}I_{37}}{N_{33}}\right)(\epsilon_8 + \epsilon_{18} + \epsilon_{27} + \epsilon_{37}) + \left(\frac{I_{33}I_8I_{19}I_{24}I_{37}}{N_{33}}\right)(\epsilon_8 + \epsilon_{19} + \epsilon_{24} + \epsilon_{37}) \end{aligned}$$

Inserting the branching ratios into the above relation gives :

$$\begin{aligned} c_{33} &= 0.4107\,(\epsilon_3 + \epsilon_{37}) + 0.5643\,(\epsilon_6 + \epsilon_{27} + \epsilon_{37}) + 0.0172\,(\epsilon_7 + \epsilon_{34} + \epsilon_{37}) + 0.0048\,(\epsilon_8 + \epsilon_{16} + \epsilon_{37}) \\ &+ 0.0029\,(\epsilon_8 + \epsilon_{18} + \epsilon_{27} + \epsilon_{37}) + 0.00006\,(\epsilon_8 + \epsilon_{19} + \epsilon_{24} + \epsilon_{37}) \end{aligned}$$

Transition 36, 4618 keV $\rightarrow$ 1778 keV, Peak at $E_\gamma = 2840\,k$eV

$$
\begin{aligned}
c_{36} = &\left(\frac{I_{36}I_2I_{37}}{N_{36}}\right)(\epsilon_2+\epsilon_{37}) + \left(\frac{I_{36}I_3I_{34}I_{37}}{N_{36}}\right)(\epsilon_3+\epsilon_{34}+\epsilon_{37}) + \left(\frac{I_{36}I_4I_{32}I_{37}}{N_{36}}\right)(\epsilon_4+\epsilon_{32}+\epsilon_{37}) \\
&+ \left(\frac{I_{36}I_5I_{29}I_{37}}{N_{36}}\right)(\epsilon_5+\epsilon_{29}+\epsilon_{37}) + \left(\frac{I_{36}I_6I_{26}I_{37}}{N_{36}}\right)(\epsilon_6+\epsilon_{26}+\epsilon_{37}) \\
&+ \left(\frac{I_{36}I_6I_{27}I_{34}I_{37}}{N_{36}}\right)(\epsilon_6+\epsilon_{27}+\epsilon_{34}+\epsilon_{37}) \\
&+ \left(\frac{I_{36}I_7I_{22}I_{37}}{N_{36}}\right)(\epsilon_7+\epsilon_{22}+\epsilon_{37}) + \left(\frac{I_{36}I_7I_{24}I_{34}I_{37}}{N_{36}}\right)(\epsilon_7+\epsilon_{24}+\epsilon_{34}+\epsilon_{37}) \\
&+ \left(\frac{I_{36}I_8I_{15}I_{37}}{N_{36}}\right)(\epsilon_8+\epsilon_{15}+\epsilon_{37}) + \left(\frac{I_{36}I_8I_{16}I_{34}I_{37}}{N_{36}}\right)(\epsilon_8+\epsilon_{16}+\epsilon_{34}+\epsilon_{37}) \\
&+ \left(\frac{I_{36}I_8I_{17}I_{29}I_{37}}{N_{36}}\right)(\epsilon_8+\epsilon_{17}+\epsilon_{29}+\epsilon_{37}) + \left(\frac{I_{36}I_8I_{18}I_{26}I_{37}}{N_{36}}\right)(\epsilon_8+\epsilon_{18}+\epsilon_{26}+\epsilon_{37}) \\
&+ \left(\frac{I_{36}I_8I_{18}I_{27}I_{34}I_{37}}{N_{36}}\right)(\epsilon_8+\epsilon_{18}+\epsilon_{27}+\epsilon_{34}+\epsilon_{37}) + \left(\frac{I_{36}I_8I_{19}I_{22}I_{37}}{N_{36}}\right)(\epsilon_8+\epsilon_{19}+\epsilon_{22}+\epsilon_{37}) \\
&+ \left(\frac{I_{36}I_8I_{19}I_{24}I_{34}I_{37}}{N_{36}}\right)(\epsilon_8+\epsilon_{19}+\epsilon_{24}+\epsilon_{34}+\epsilon_{37}) + \left(\frac{I_{36}I_9I_{12}I_{37}}{N_{36}}\right)(\epsilon_9+\epsilon_{12}+\epsilon_{37}) \\
&= 0.8142\,(\epsilon_2+\epsilon_{37}) + 0.047\,(\epsilon_3+\epsilon_{34}+\epsilon_{37}) + 0.0027\,(\epsilon_4+\epsilon_{32}+\epsilon_{37}) \\
&+ 0.0006\,(\epsilon_5+\epsilon_{29}+\epsilon_{37}) + 0.0213\,(\epsilon_6+\epsilon_{26}+\epsilon_{37}) + 0.0647\,(\epsilon_6+\epsilon_{27}+\epsilon_{34}+\epsilon_{37}) \\
&+ 0.0328\,(\epsilon_7+\epsilon_{22}+\epsilon_{37}) + 0.0020\,(\epsilon_7+\epsilon_{24}+\epsilon_{34}+\epsilon_{37}) \\
&+ 0.0540\,(\epsilon_8+\epsilon_{15}+\epsilon_{37}) + 0.0005\,(\epsilon_8+\epsilon_{16}+\epsilon_{34}+\epsilon_{37}) \\
&+ 0.0036\,(\epsilon_8+\epsilon_{17}+\epsilon_{29}+\epsilon_{37}) + 0.0001\,(\epsilon_8+\epsilon_{18}+\epsilon_{26}+\epsilon_{37}) \\
&+ 0.0003\,(\epsilon_8+\epsilon_{18}+\epsilon_{27}+\epsilon_{34}+\epsilon_{37}) + 0.0001\,(\epsilon_8+\epsilon_{19}+\epsilon_{22}+\epsilon_{37}) \\
&+ 0.000006\,(\epsilon_8+\epsilon_{19}+\epsilon_{24}+\epsilon_{34}+\epsilon_{37}) + 0.0138\,(\epsilon_9+\epsilon_{12}+\epsilon_{37})
\end{aligned}
$$

Transition 37, 1778 keV $\rightarrow$ 0 keV, Peak at $E_\gamma = 1778\,k\mathrm{eV}$

$$
\begin{aligned}
c_{37} = {} & \left(\frac{I_{37}I_1}{N_{37}}\right)\epsilon_1 + \left(\frac{I_{37}I_2I_{36}}{N_{37}}\right)(\epsilon_2+\epsilon_{36}) + \left(\frac{I_{37}I_3I_{33}}{N_{37}}\right)(\epsilon_3+\epsilon_{33}) + \left(\frac{I_3I_{34}I_{36}I_{37}}{N_{37}}\right)(\epsilon_3+\epsilon_{34}+\epsilon_{36}) \\
& + \left(\frac{I_4I_{31}I_{37}}{N_{37}}\right)(\epsilon_4+\epsilon_{31}) + \left(\frac{I_4I_{32}I_{36}I_{37}}{N_{37}}\right)(\epsilon_4+\epsilon_{32}+\epsilon_{36}) + \left(\frac{I_5I_{28}I_{37}}{N_{37}}\right)(\epsilon_5+\epsilon_{28}) \\
& + \left(\frac{I_5I_{29}I_{36}I_{37}}{N_{37}}\right)(\epsilon_5+\epsilon_{29}+\epsilon_{36}) + \left(\frac{I_6I_{25}I_{37}}{N_{37}}\right)(\epsilon_6+\epsilon_{25}) + \left(\frac{I_6I_{26}I_{36}I_{37}}{N_{37}}\right)(\epsilon_6+\epsilon_{26}+\epsilon_{36}) \\
& + \left(\frac{I_6I_{27}I_{33}I_{37}}{N_{37}}\right)(\epsilon_6+\epsilon_{27}+\epsilon_{33}) + \left(\frac{I_6I_{27}I_{34}I_{36}I_{37}}{N_{37}}\right)(\epsilon_6+\epsilon_{27}+\epsilon_{34}+\epsilon_{36}) + \left(\frac{I_7I_{21}I_{37}}{N_{37}}\right)(\epsilon_7+\epsilon_{21}) \\
& + \left(\frac{I_7I_{22}I_{36}I_{37}}{N_{37}}\right)(\epsilon_7+\epsilon_{22}+\epsilon_{36}) + \left(\frac{I_7I_{23}I_{35}I_{37}}{N_{37}}\right)(\epsilon_7+\epsilon_{23}+\epsilon_{35}) + \left(\frac{I_7I_{24}I_{33}I_{37}}{N_{37}}\right)(\epsilon_7+\epsilon_{24}+\epsilon_{33}) \\
& + \left(\frac{I_7I_{24}I_{34}I_{36}I_{37}}{N_{37}}\right)(\epsilon_7+\epsilon_{24}+\epsilon_{34}+\epsilon_{36}) + \left(\frac{I_8I_{14}I_{37}}{N_{37}}\right)(\epsilon_8+\epsilon_{14}) + \left(\frac{I_8I_{15}I_{36}I_{37}}{N_{37}}\right)(\epsilon_8+\epsilon_{15}+\epsilon_{36}) \\
& + \left(\frac{I_8I_{16}I_{33}I_{37}}{N_{37}}\right)(\epsilon_8+\epsilon_{16}+\epsilon_{33}) + \left(\frac{I_8I_{16}I_{34}I_{36}I_{37}}{N_{37}}\right)(\epsilon_8+\epsilon_{16}+\epsilon_{34}+\epsilon_{36}) \\
& + \left(\frac{I_8I_{17}I_{28}I_{37}}{N_{37}}\right)(\epsilon_8+\epsilon_{17}+\epsilon_{28}) + \left(\frac{I_8I_{17}I_{29}I_{36}I_{37}}{N_{37}}\right)(\epsilon_8+\epsilon_{17}+\epsilon_{29}+\epsilon_{36}) \\
& + \left(\frac{I_8I_{18}I_{25}I_{37}}{N_{37}}\right)(\epsilon_8+\epsilon_{18}+\epsilon_{25}) + \left(\frac{I_8I_{18}I_{26}I_{36}I_{37}}{N_{37}}\right)(\epsilon_8+\epsilon_{18}+\epsilon_{26}+\epsilon_{36}) \\
& + \left(\frac{I_8I_{18}I_{27}I_{33}I_{37}}{N_{37}}\right)(\epsilon_8+\epsilon_{18}+\epsilon_{27}+\epsilon_{33}) + \left(\frac{I_8I_{18}I_{27}I_{34}I_{36}I_{37}}{N_{37}}\right)(\epsilon_8+\epsilon_{18}+\epsilon_{27}+\epsilon_{34}+\epsilon_{36}) \\
& + \left(\frac{I_8I_{19}I_{21}I_{37}}{N_{37}}\right)(\epsilon_8+\epsilon_{19}+\epsilon_{21}) + \left(\frac{I_8I_{19}I_{22}I_{36}I_{37}}{N_{37}}\right)(\epsilon_8+\epsilon_{19}+\epsilon_{22}+\epsilon_{36}) \\
& + \left(\frac{I_8I_{19}I_{23}I_{35}I_{37}}{N_{37}}\right)(\epsilon_8+\epsilon_{19}+\epsilon_{23}+\epsilon_{35}) + \left(\frac{I_8I_{19}I_{24}I_{33}I_{37}}{N_{37}}\right)(\epsilon_8+\epsilon_{19}+\epsilon_{24}+\epsilon_{33}) \\
& + \left(\frac{I_8I_{19}I_{24}I_{34}I_{36}I_{37}}{N_{37}}\right)(\epsilon_8+\epsilon_{19}+\epsilon_{24}+\epsilon_{34}+\epsilon_{36}) + \left(\frac{I_9I_{11}I_{37}}{N_{37}}\right)(\epsilon_9+\epsilon_{11}) \\
& + \left(\frac{I_9I_{12}I_{36}I_{37}}{N_{37}}\right)(\epsilon_9+\epsilon_{12}+\epsilon_{36}) + \left(\frac{I_9I_{13}I_{35}I_{37}}{N_{37}}\right)(\epsilon_9+\epsilon_{13}+\epsilon_{35}) \\
& = 0.7975\epsilon_1 + 0.052\,(\epsilon_2+\epsilon_{36}) + 0.225\,(\epsilon_3+\epsilon_{33}) + 0.003\,(\epsilon_3+\epsilon_{34}+\epsilon_{36}) + 0.0017\,(\epsilon_4+\epsilon_{31}) \\
& + 0.0002\,(\epsilon_4+\epsilon_{32}+\epsilon_{36}) + 0.0031\,(\epsilon_5+\epsilon_{28}) + 0.00004\,(\epsilon_5+\epsilon_{29}+\epsilon_{36}) \\
& + 0.0669\,(\epsilon_6+\epsilon_{25}) + 0.0014\,(\epsilon_6+\epsilon_{26}+\epsilon_{36}) + 0.0308\,(\epsilon_6+\epsilon_{27}+\epsilon_{33}) \\
& + 0.0041\,(\epsilon_6+\epsilon_{27}+\epsilon_{34}+\epsilon_{36}) + 0.0025\,(\epsilon_7+\epsilon_{21}) + 0.0021\,(\epsilon_7+\epsilon_{22}+\epsilon_{36}) \\
& + 0.0018\,(\epsilon_7+\epsilon_{23}+\epsilon_{35}) + 0.0009\,(\epsilon_7+\epsilon_{24}+\epsilon_{33}) + 0.0001\,(\epsilon_7+\epsilon_{24}+\epsilon_{34}+\epsilon_{36}) \\
& + 0.0032\,(\epsilon_8+\epsilon_{14}) + 0.0034\,(\epsilon_8+\epsilon_{15}+\epsilon_{36}) + 0.0002\,(\epsilon_8+\epsilon_{16}+\epsilon_{33}) + 0.00003\,(\epsilon_8+\epsilon_{16}+\epsilon_{34}+\epsilon_{36}) \\
& + 0.0018\,(\epsilon_8+\epsilon_{17}+\epsilon_{28}) + 0.00002\,(\epsilon_8+\epsilon_{17}+\epsilon_{29}+\epsilon_{36}) + 0.0003\,(\epsilon_8+\epsilon_{18}+\epsilon_{25}) \\
& + 0.000007\,(\epsilon_8+\epsilon_{18}+\epsilon_{26}+\epsilon_{36}) + 0.0002\,(\epsilon_8+\epsilon_{18}+\epsilon_{27}+\epsilon_{33}) + 0.00002\,(\epsilon_8+\epsilon_{18}+\epsilon_{27}+\epsilon_{34}+\epsilon_{36}) \\
& + 0.000008\,(\epsilon_8+\epsilon_{19}+\epsilon_{21}) + 0.000007\,(\epsilon_8+\epsilon_{19}+\epsilon_{22}+\epsilon_{36}) + 0.000006\,(\epsilon_8+\epsilon_{19}+\epsilon_{23}+\epsilon_{35}) \\
& + 0.000003\,(\epsilon_8+\epsilon_{19}+\epsilon_{24}+\epsilon_{33}) + 0.0000004\,(\epsilon_8+\epsilon_{19}+\epsilon_{24}+\epsilon_{34}+\epsilon_{36}) + 0.0004\,(\epsilon_9+\epsilon_{11}) \\
& + 0.0009\,(\epsilon_9+\epsilon_{12}+\epsilon_{36}) + 0.0006\,(\epsilon_9+\epsilon_{13}+\epsilon_{35})
\end{aligned}
$$

Summing corrections for $^{27}Al(p,\gamma)^{28}Si$ at $E_p = 406\,k\text{eV}$

Analogous to the previous section, the summing corrections for $^{27}Al(p,\gamma)^{28}Si$ at $E_p = 406\,k\text{eV}$ are calculated, based on figure A.2.

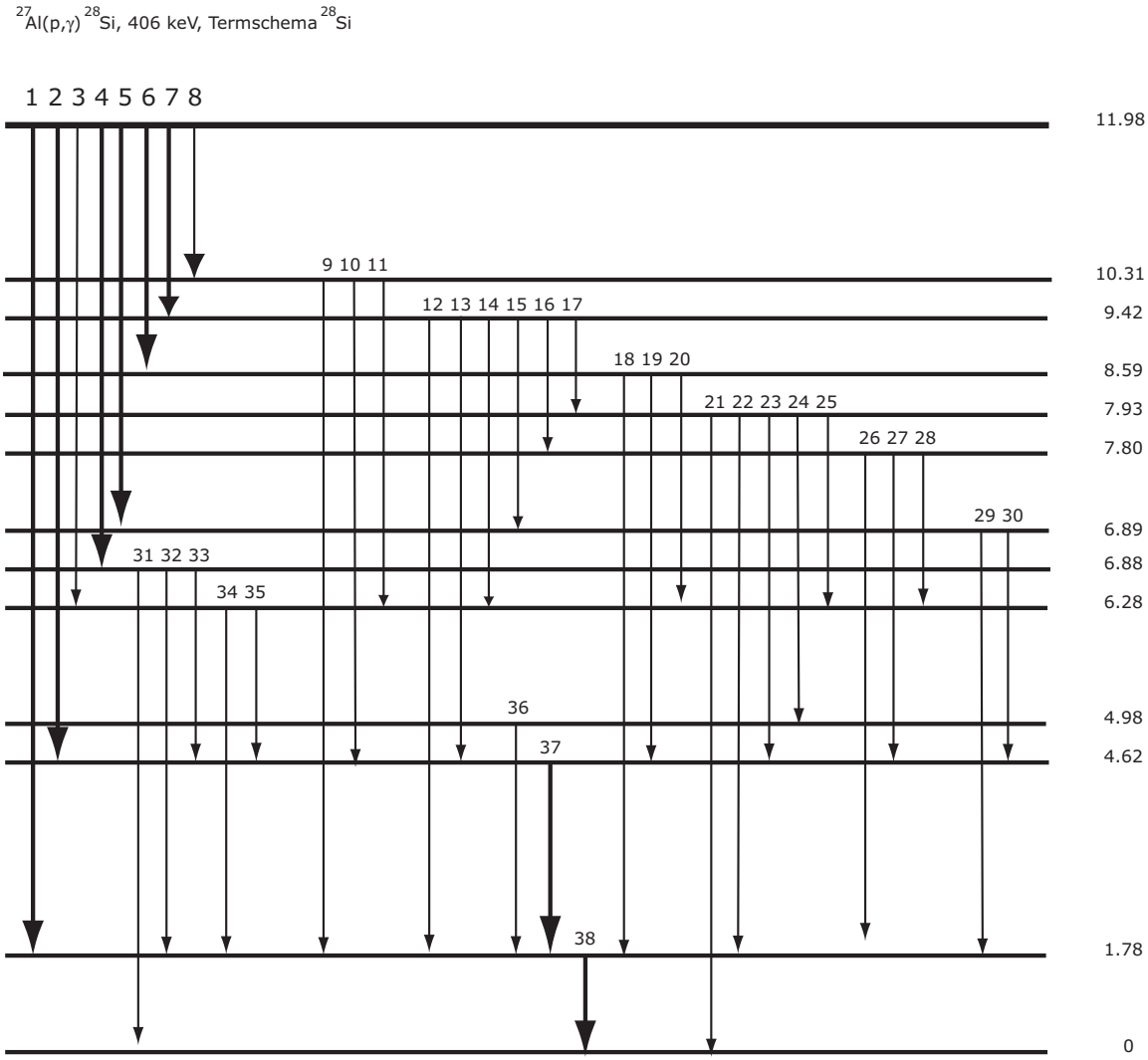

Figure A.2: Simplified decay scheme of ^{28}Si at $E_p = 406\,k\text{eV}$.

Transition 1, $11977\,k\text{eV} \rightarrow 1778\,k\text{eV}$, Peak at $E_\gamma = 10198\,k\text{eV}$

$$\begin{aligned} c_1 &= \left(\frac{I_1 I_{38}}{N_1}\right)\epsilon_{38} \\ &= \epsilon_{38} \end{aligned}$$

Transition 2, 11977 keV $\rightarrow$ 4618 keV, Peak at $E_\gamma = 7360\,k\text{eV}$

$$\begin{aligned} c_2 &= \left(\frac{I_2 I_{37} I_{38}}{N_2}\right)(\epsilon_{37} + \epsilon_{38}) \\ &= \epsilon_{37} + \epsilon_{38} \end{aligned}$$

Transition 4, 11977 keV $\rightarrow$ 6878 keV, Peak at $E_\gamma = 5099\,k\text{eV}$

$$\begin{aligned} c_4 &= \left(\frac{I_4 I_{31}}{N_4}\right)\epsilon_{31} + \left(\frac{I_4 I_{32} I_{38}}{N_4}\right)(\epsilon_{32} + \epsilon_{38}) + \left(\frac{I_4 I_{33} I_{37} I_{38}}{N_4}\right)(\epsilon_{33} + \epsilon_{37} + \epsilon_{38}) \\ &= 0.7\epsilon_{31} + 0.273\,(\epsilon_{32} + \epsilon_{38}) + 0.027\,(\epsilon_{33} + \epsilon_{37} + \epsilon_{38}) \end{aligned}$$

Transition 5, 11977 keV $\rightarrow$ 6888 keV, Peak at $E_\gamma = 5089\,k\text{eV}$

$$\begin{aligned} c_5 &= \left(\frac{I_5 I_{29} I_{38}}{N_5}\right)(\epsilon_{29} + \epsilon_{38}) + \left(\frac{I_5 I_{30} I_{37} I_{38}}{N_5}\right)(\epsilon_{30} + \epsilon_{37} + \epsilon_{38}) \\ &= 0.9871\,(\epsilon_{29} + \epsilon_{38}) + 0.0213\,(\epsilon_{30} + \epsilon_{37} + \epsilon_{38}) \end{aligned}$$

Transition 6, 11977 keV $\rightarrow$ 8588 keV, Peak at $E_\gamma = 3389\,k\text{eV}$

$$\begin{aligned} c_6 &= \left(\frac{I_6 I_{38}}{N_6}\right)(\epsilon_{18} + \epsilon_{38}) + \left(\frac{I_6 I_{19} I_{37} I_{38}}{N_6}\right)(\epsilon_{19} + \epsilon_{37} + \epsilon_{38}) \\ &+ \left(\frac{I_6 I_{20} I_{34} I_{38}}{N_6}\right)(\epsilon_{20} + \epsilon_{34} + \epsilon_{38}) + \left(\frac{I_6 I_{20} I_{35} I_{37} I_{38}}{N_6}\right)(\epsilon_{20} + \epsilon_{35} + \epsilon_{37} + \epsilon_{38}) \\ &= 0.887\,(\epsilon_{18} + \epsilon_{38}) + 0.043\,(\epsilon_{19} + \epsilon_{37} + \epsilon_{38}) + 0.0606\,(\epsilon_{20} + \epsilon_{34} + \epsilon_{38}) + 0.0081\,(\epsilon_{20} + \epsilon_{35} + \epsilon_{37} + \epsilon_{38}) \end{aligned}$$

Transition 7, 11977 keV $\rightarrow$ 9417 keV, Peak at $E_\gamma = 2560\,k$eV

$$
\begin{aligned}
c_7 = & \left(\frac{I_7 I_{12} I_{38}}{N_7}\right)(\epsilon_{12}+\epsilon_{38}) + \left(\frac{I_7 I_{13} I_{37} I_{38}}{N_7}\right)(\epsilon_{13}+\epsilon_{37}+\epsilon_{38}) + \left(\frac{I_7 I_{14} I_{34} I_{38}}{N_7}\right)(\epsilon_{14}+\epsilon_{34}+\epsilon_{38}) \\
& + \left(\frac{I_7 I_{14} I_{35} I_{37} I_{38}}{N_7}\right)(\epsilon_{14}+\epsilon_{35}+\epsilon_{37}+\epsilon_{38}) + \left(\frac{I_7 I_{15} I_{29} I_{38}}{N_7}\right)(\epsilon_{15}+\epsilon_{29}+\epsilon_{38}) \\
& + \left(\frac{I_7 I_{15} I_{30} I_{37} I_{38}}{N_7}\right)(\epsilon_{15}+\epsilon_{30}+\epsilon_{37}+\epsilon_{38}) + \left(\frac{I_7 I_{16} I_{28} I_{38}}{N_7}\right)(\epsilon_{16}+\epsilon_{28}+\epsilon_{38}) \\
& + \left(\frac{I_7 I_{16} I_{27} I_{37} I_{38}}{N_7}\right)(\epsilon_{16}+\epsilon_{27}+\epsilon_{37}+\epsilon_{38}) + \left(\frac{I_7 I_{16} I_{28} I_{34} I_{38}}{N_7}\right)(\epsilon_{16}+\epsilon_{28}+\epsilon_{34}+\epsilon_{38}) \\
& + \left(\frac{I_7 I_{16} I_{28} I_{35} I_{37} I_{38}}{N_7}\right)(\epsilon_{16}+\epsilon_{28}+\epsilon_{35}+\epsilon_{37}+\epsilon_{38}) + \left(\frac{I_7 I_{17} I_{21}}{N_7}\right)(\epsilon_{17}+\epsilon_{21}) \\
& + \left(\frac{I_7 I_{17} I_{22} I_{38}}{N_7}\right)(\epsilon_{17}+\epsilon_{22}+\epsilon_{38}) \\
& + \left(\frac{I_7 I_{17} I_{23} I_{37} I_{38}}{N_7}\right)(\epsilon_{17}+\epsilon_{23}+\epsilon_{37}+\epsilon_{38}) + \left(\frac{I_7 I_{17} I_{24} I_{36} I_{38}}{N_7}\right)(\epsilon_{17}+\epsilon_{24}+\epsilon_{36}+\epsilon_{38}) \\
& + \left(\frac{I_7 I_{17} I_{25} I_{34} I_{38}}{N_7}\right)(\epsilon_{17}+\epsilon_{25}+\epsilon_{34}+\epsilon_{38}) + \left(\frac{I_7 I_{17} I_{25} I_{35} I_{37} I_{38}}{N_7}\right)(\epsilon_{17}+\epsilon_{25}+\epsilon_{35}+\epsilon_{37}+\epsilon_{38}) \\
& = 0.3310\,(\epsilon_{12}+\epsilon_{38}) + 0.361\,(\epsilon_{13}+\epsilon_{37}+\epsilon_{38}) + 0.0273\,(\epsilon_{14}+\epsilon_{34}+\epsilon_{38}) + 0.0037\,(\epsilon_{14}+\epsilon_{35}+\epsilon_{37}+\epsilon_{38}) \\
& + 0.1846\,(\epsilon_{15}+\epsilon_{29}+\epsilon_{38}) + 0.0024\,(\epsilon_{15}+\epsilon_{30}+\epsilon_{37}+\epsilon_{38}) + 0.0366\,(\epsilon_{16}+\epsilon_{28}+\epsilon_{38}) \\
& + 0.0007\,(\epsilon_{16}+\epsilon_{27}+\epsilon_{37}+\epsilon_{38}) + 0.0168\,(\epsilon_{16}+\epsilon_{28}+\epsilon_{34}+\epsilon_{38}) + 0.0022\,(\epsilon_{16}+\epsilon_{28}+\epsilon_{35}+\epsilon_{37}+\epsilon_{38}) \\
& + 0.0125\,(\epsilon_{17}+\epsilon_{21}) + 0.0008\,(\epsilon_{17}+\epsilon_{22}+\epsilon_{38}) + 0.0007\,(\epsilon_{17}+\epsilon_{23}+\epsilon_{37}+\epsilon_{38}) \\
& + 0.0006\,(\epsilon_{17}+\epsilon_{24}+\epsilon_{36}+\epsilon_{38}) + 0.0004\,(\epsilon_{17}+\epsilon_{25}+\epsilon_{34}+\epsilon_{38}) + 0.00004\,(\epsilon_{17}+\epsilon_{25}+\epsilon_{35}+\epsilon_{37}+\epsilon_{38})
\end{aligned}
$$

Transition 37, 4618 keV $\rightarrow$ 1778 keV, Peak at $E_\gamma = 2840\,k$eV

$$
\begin{aligned}
c_{37} = & \left(\frac{I_{37}I_2I_{38}}{N_{37}}\right)(\epsilon_2+\epsilon_{38}) + \left(\frac{I_{37}I_3I_{35}I_{38}}{N_{37}}\right)(\epsilon_3+\epsilon_{35}+\epsilon_{38}) + \left(\frac{I_{37}I_4I_{33}I_{38}}{N_{37}}\right)(\epsilon_4+\epsilon_{33}+\epsilon_{38}) \\
& + \left(\frac{I_{37}I_5I_{30}I_{38}}{N_{37}}\right)(\epsilon_5+\epsilon_{30}+\epsilon_{38}) + \left(\frac{I_{37}I_6I_{19}I_{38}}{N_{37}}\right)(\epsilon_6+\epsilon_{19}+\epsilon_{38}) \\
& + \left(\frac{I_{37}I_6I_{20}I_{35}I_{38}}{N_{37}}\right)(\epsilon_6+\epsilon_{20}+\epsilon_{35}+\epsilon_{38}) + \left(\frac{I_{37}I_7I_{13}I_{38}}{N_{37}}\right)(\epsilon_7+\epsilon_{13}+\epsilon_{38}) \\
& + \left(\frac{I_{37}I_7I_{16}I_{27}I_{38}}{N_{37}}\right)(\epsilon_7+\epsilon_{16}+\epsilon_{27}+\epsilon_{38}) + \left(\frac{I_{37}I_7I_{16}I_{28}I_{35}I_{38}}{N_{37}}\right)(\epsilon_7+\epsilon_{16}+\epsilon_{28}+\epsilon_{35}+\epsilon_{38}) \\
& + \left(\frac{I_{37}I_7I_{14}I_{35}I_{38}}{N_{37}}\right)(\epsilon_7+\epsilon_{14}+\epsilon_{35}+\epsilon_{38}) \\
& + \left(\frac{I_{37}I_7I_{15}I_{30}I_{38}}{N_{37}}\right)(\epsilon_7+\epsilon_{15}+\epsilon_{30}+\epsilon_{38}) \\
& + \left(\frac{I_{37}I_7I_{17}I_{23}I_{38}}{N_{37}}\right)(\epsilon_7+\epsilon_{17}+\epsilon_{23}+\epsilon_{38}) \\
& + \left(\frac{I_{37}I_8I_{10}I_{38}}{N_{37}}\right)(\epsilon_8+\epsilon_{10}+\epsilon_{38}) + \left(\frac{I_{37}I_7I_{17}I_{25}I_{35}I_{38}}{N_{37}}\right)(\epsilon_7+\epsilon_{17}+\epsilon_{25}+\epsilon_{35}+\epsilon_{38}) \\
& + \left(\frac{I_{37}I_8I_{11}I_{25}I_{38}}{N_{37}}\right)(\epsilon_8+\epsilon_{11}+\epsilon_{25}+\epsilon_{38}) \\
& = 0.954961\,(\epsilon_2+\epsilon_{38}) + 0.002539\,(\epsilon_3+\epsilon_{35}+\epsilon_{38}) + 0.004430\,(\epsilon_4+\epsilon_{33}+\epsilon_{38}) \\
& + 0.000989\,(\epsilon_5+\epsilon_{30}+\epsilon_{38}) + 0.003354\,(\epsilon_6+\epsilon_{19}+\epsilon_{38}) + 0.000635\,(\epsilon_6+\epsilon_{20}+\epsilon_{35}+\epsilon_{38}) \\
& + 0.013595\,(\epsilon_7+\epsilon_{13}+\epsilon_{38}) + 0.000138\,(\epsilon_7+\epsilon_{14}+\epsilon_{35}+\epsilon_{38}) \\
& + 0.000091\,(\epsilon_7+\epsilon_{15}+\epsilon_{30}+\epsilon_{38}) + 0.000028\,(\epsilon_7+\epsilon_{16}+\epsilon_{27}+\epsilon_{38}) \\
& + 0.000085\,(\epsilon_7+\epsilon_{16}+\epsilon_{28}+\epsilon_{35}+\epsilon_{38}) + 0.000027\,(\epsilon_7+\epsilon_{17}+\epsilon_{23}+\epsilon_{38}) \\
& + 0.000002\,(\epsilon_7+\epsilon_{17}+\epsilon_{25}+\epsilon_{35}+\epsilon_{38}) + 0.012778\,(\epsilon_8+\epsilon_{10}+\epsilon_{38}) \\
& + 0.006348\,(\epsilon_8+\epsilon_{11}+\epsilon_{25}+\epsilon_{38})
\end{aligned}
$$

Transition 38, 1778 keV $\rightarrow$ 0 keV, Peak at $E_\gamma = 1778\,k$eV

$$
\begin{aligned}
c_{38} = & \left(\frac{I_{38}I_1}{N_{38}}\right)\epsilon_1 + \left(\frac{I_{38}I_2I_{37}}{N_{38}}\right)(\epsilon_2+\epsilon_{37}) + \left(\frac{I_{38}I_3I_{34}}{N_{38}}\right)(\epsilon_3+\epsilon_{34}) + \left(\frac{I_3I_{35}I_{37}I_{38}}{N_{38}}\right)(\epsilon_3+\epsilon_{35}+\epsilon_{37}) \\
& + \left(\frac{I_4I_{32}I_{38}}{N_{38}}\right)(\epsilon_4+\epsilon_{32}) + \left(\frac{I_4I_{33}I_{37}I_{38}}{N_{38}}\right)(\epsilon_4+\epsilon_{33}+\epsilon_{37}) + \left(\frac{I_5I_{29}I_{38}}{N_{38}}\right)(\epsilon_5+\epsilon_{29}) \\
& + \left(\frac{I_5I_{30}I_{37}I_{38}}{N_{38}}\right)(\epsilon_5+\epsilon_{30}+\epsilon_{37}) + \left(\frac{I_6I_{18}I_{38}}{N_{38}}\right)(\epsilon_6+\epsilon_{18}) + \left(\frac{I_6I_{19}I_{37}I_{38}}{N_{38}}\right)(\epsilon_6+\epsilon_{19}+\epsilon_{37}) \\
& + \left(\frac{I_6I_{20}I_{34}I_{38}}{N_{38}}\right)(\epsilon_6+\epsilon_{20}+\epsilon_{34}) + \left(\frac{I_6I_{20}I_{35}I_{37}I_{38}}{N_{38}}\right)(\epsilon_6+\epsilon_{20}+\epsilon_{35}+\epsilon_{37}) \\
& + \left(\frac{I_7I_{12}I_{38}}{N_{38}}\right)(\epsilon_7+\epsilon_{12}) + \left(\frac{I_7I_{13}I_{37}I_{38}}{N_{38}}\right)(\epsilon_7+\epsilon_{13}+\epsilon_{37}) + \left(\frac{I_7I_{14}I_{34}I_{38}}{N_{38}}\right)(\epsilon_7+\epsilon_{14}+\epsilon_{34}) \\
& + \left(\frac{I_7I_{14}I_{35}I_{37}I_{38}}{N_{38}}\right)(\epsilon_7+\epsilon_{14}+\epsilon_{35}+\epsilon_{37}) + \left(\frac{I_7I_{15}I_{29}I_{38}}{N_{38}}\right)(\epsilon_7+\epsilon_{15}+\epsilon_{29}) \\
& + \left(\frac{I_7I_{15}I_{30}I_{37}I_{38}}{N_{38}}\right)(\epsilon_7+\epsilon_{15}+\epsilon_{30}+\epsilon_{37}) + \left(\frac{I_7I_{16}I_{26}I_{38}}{N_{38}}\right)(\epsilon_7+\epsilon_{16}+\epsilon_{26}) \\
& + \left(\frac{I_7I_{16}I_{27}I_{37}I_{38}}{N_{38}}\right)(\epsilon_7+\epsilon_{16}+\epsilon_{27}+\epsilon_{37}) + \left(\frac{I_7I_{16}I_{28}I_{34}I_{38}}{N_{38}}\right)(\epsilon_7+\epsilon_{16}+\epsilon_{28}+\epsilon_{34}) \\
& + \left(\frac{I_7I_{16}I_{28}I_{35}I_{37}I_{38}}{N_{38}}\right)(\epsilon_7+\epsilon_{16}+\epsilon_{28}+\epsilon_{35}+\epsilon_{37}) + \left(\frac{I_7I_{17}I_{22}I_{37}I_{38}}{N_{38}}\right)(\epsilon_7+\epsilon_{17}+\epsilon_{22}+\epsilon_{37}) \\
& + \left(\frac{I_7I_{17}I_{23}I_{37}I_{38}}{N_{38}}\right)(\epsilon_7+\epsilon_{17}+\epsilon_{23}+\epsilon_{37}) + \left(\frac{I_7I_{17}I_{24}I_{36}I_{38}}{N_{38}}\right)(\epsilon_7+\epsilon_{17}+\epsilon_{24}+\epsilon_{36}) \\
& + \left(\frac{I_7I_{17}I_{25}I_{34}I_{38}}{N_{38}}\right)(\epsilon_7+\epsilon_{17}+\epsilon_{25}+\epsilon_{34}) + \left(\frac{I_7I_{17}I_{25}I_{35}I_{37}I_{38}}{N_{38}}\right)(\epsilon_7+\epsilon_{17}+\epsilon_{25}+\epsilon_{35}+\epsilon_{37}) \\
& + \left(\frac{I_8I_9I_{38}}{N_{38}}\right)(\epsilon_8+\epsilon_9) + \left(\frac{I_8I_{10}I_{37}I_{38}}{N_{38}}\right)(\epsilon_8+\epsilon_{10}+\epsilon_{37}) \\
& + \left(\frac{I_8I_{11}I_{34}I_{38}}{N_{38}}\right)(\epsilon_8+\epsilon_{11}+\epsilon_{35}) + \left(\frac{I_8I_{11}I_{35}I_{37}I_{38}}{N_{38}}\right)(\epsilon_8+\epsilon_{11}+\epsilon_{35}+\epsilon_{37}) \\
& = 0.02430\epsilon_1 + 0.75000\,(\epsilon_2+\epsilon_{37}) + 0.01491\,(\epsilon_3+\epsilon_{34}) + 0.00199\,(\epsilon_3+\epsilon_{35}+\epsilon_{37}) \\
& + 0.03518\,(\epsilon_4+\epsilon_{32}) + 0.00348\,(\epsilon_4+\epsilon_{33}+\epsilon_{37}) + 0.05943\,(\epsilon_5+\epsilon_{29}) \\
& + 0.00078\,(\epsilon_5+\epsilon_{30}+\epsilon_{37}) + 0.05434\,(\epsilon_6+\epsilon_{18}) + 0.00263\,(\epsilon_6+\epsilon_{19}+\epsilon_{37}) \\
& + 0.00373\,(\epsilon_6+\epsilon_{20}+\epsilon_{34}) + 0.00050\,(\epsilon_6+\epsilon_{20}+\epsilon_{35}+\epsilon_{37}) \\
& + 0.00979\,(\epsilon_7+\epsilon_{12}) + 0.01068\,(\epsilon_7+\epsilon_{13}+\epsilon_{37}) \\
& + 0.00081\,(\epsilon_7+\epsilon_{14}+\epsilon_{34}) + 0.00011\,(\epsilon_7+\epsilon_{14}+\epsilon_{35}+\epsilon_{37}) \\
& + 0.00546\,(\epsilon_7+\epsilon_{15}+\epsilon_{29}) \\
& + 0.00007\,(\epsilon_7+\epsilon_{15}+\epsilon_{30}+\epsilon_{37}) + 0.00108\,(\epsilon_7+\epsilon_{16}+\epsilon_{26}) \\
& + 0.00002\,(\epsilon_7+\epsilon_{16}+\epsilon_{27}+\epsilon_{37}) + 0.00050\,(\epsilon_7+\epsilon_{16}+\epsilon_{28}+\epsilon_{34}) \\
& + 0.00007\,(\epsilon_7+\epsilon_{16}+\epsilon_{28}+\epsilon_{35}+\epsilon_{37}) + 0.00002\,(\epsilon_7+\epsilon_{17}+\epsilon_{22}+\epsilon_{37}) \\
& + 0.00002\,(\epsilon_7+\epsilon_{17}+\epsilon_{23}+\epsilon_{37}) + 0.00002\,(\epsilon_7+\epsilon_{17}+\epsilon_{24}+\epsilon_{36}) \\
& + 0.00001\,(\epsilon_7+\epsilon_{17}+\epsilon_{25}+\epsilon_{34}) + 0.000001\,(\epsilon_7+\epsilon_{17}+\epsilon_{25}+\epsilon_{35}+\epsilon_{37}) \\
& + 0.00201\,(\epsilon_8+\epsilon_9) + 0.01004\,(\epsilon_8+\epsilon_{10}+\epsilon_{37}) \\
& + 0.00708\,(\epsilon_8+\epsilon_{11}+\epsilon_{35}) + 0.00095\,(\epsilon_8+\epsilon_{11}+\epsilon_{35}+\epsilon_{37})
\end{aligned}
$$

Summing corrections for $^{20}Ne(p,\gamma)^{21}Na$ at $E_p = 1169\,k\text{eV}$

Here the summing corrections for $^{20}Ne(p,\gamma)^{21}Na$ at $E_p = 1169\,k\text{eV}$ are calculated, based on figure A.3:

Transition 1, $3544\,k\text{eV} \rightarrow 0\,k\text{eV}$, Peak at $E_\gamma = 3544\,k\text{eV}$

$$\begin{aligned} c_1 &= \left(\frac{I_1}{N_1}\right)\epsilon_1 \\ &= \epsilon_1 \end{aligned}$$

Transition 2, $3544\,k\text{eV} \rightarrow 331\,k\text{eV}$, Peak at $E_\gamma = 3213\,k\text{eV}$

$$\begin{aligned} c_2 &= \left(\frac{I_2 I_6}{N_2}\right)\epsilon_6 \\ &= \epsilon_6 \end{aligned}$$

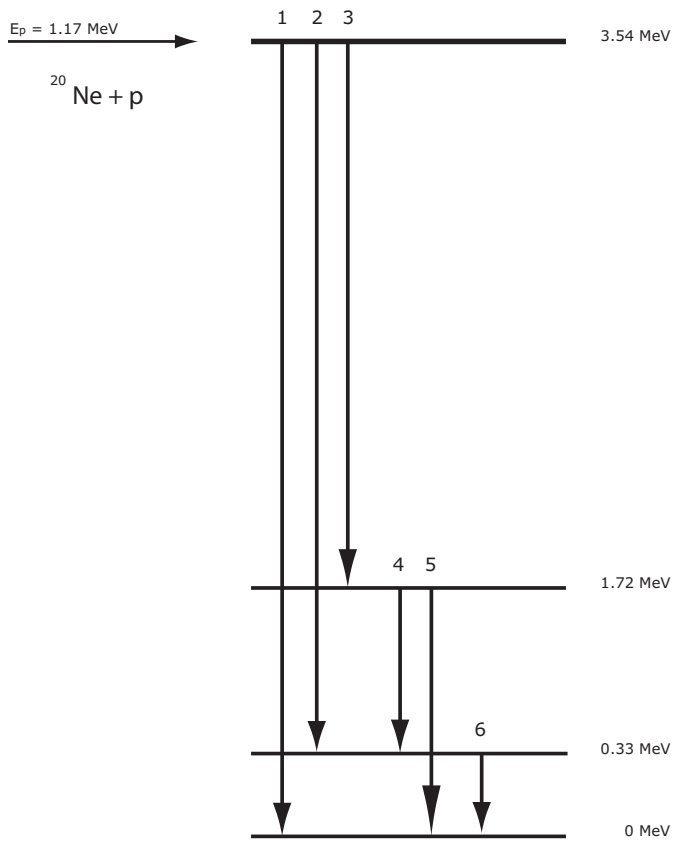

Figure A.3: Simplified decay scheme of ^{21}Na at $E_p = 1169\,k\text{eV}$

Transition 3, $3544\,k\text{eV} \rightarrow 1716\,k\text{eV}$, Peak at $E_\gamma = 1828\,k\text{eV}$

$$
\begin{aligned}
c_3 &= \left(\frac{I_3 I_4 I_6}{N_3}\right)(\epsilon_4 + \epsilon_6) \\
&= \epsilon_4 + \epsilon_6
\end{aligned}
$$

Transition 4, $1716\,k\text{eV} \rightarrow 0\,k\text{eV}$, Peak at $E_\gamma = 1716\,k\text{eV}$

$$
\begin{aligned}
c_4 &= \left(\frac{I_3 I_4 I_6}{N_4}\right)(\epsilon_3 + \epsilon_6) \\
&= \epsilon_4 + \epsilon_6
\end{aligned}
$$

Transition 5, $1716\,k\text{eV} \rightarrow 331\,k\text{eV}$, Peak at $E_\gamma = 1385\,k\text{eV}$

$$
\begin{aligned}
c_5 &= \left(\frac{I_5 I_3}{N_3}\right)\epsilon_5 \\
&= \epsilon_5
\end{aligned}
$$

Transition 6, $331\,k\text{eV} \rightarrow 0\,k\text{eV}$, Peak at $E_\gamma = 331\,k\text{eV}$

$$
\begin{aligned}
c_6 &= \left(\frac{I_2 I_6}{N_6}\right)\epsilon_2 + \left(\frac{I_3 I_4 I_6}{N_6}\right)(\epsilon_3 + \epsilon_4) \\
&= 0.8291\epsilon_2 + 0.1709\,(\epsilon_3 + \epsilon_4)
\end{aligned}
$$

Appendix B

Appendix

B.1 Determination of mass absorption coefficients

In general the mass absorption is defined as :

$$I/I_0 = e^{-(\mu/\rho)x} \tag{B.1}$$

where μ/ρ is the mass absorption coefficient while x is the mass thickness. The mass thickness is defined as following, where ρ is mass density and t the material thickness.

$$x = \rho t \tag{B.2}$$

Tables of the mass absorption coefficients exist for the elements constituting the materials used.(see http://physics.nist.gov/PhysRefData/XrayMassCoef/cover.html). Unfortunately, the energy intervals are to big to allow a precise calculation of the mass absorption. Therefore the table data was plotted and fitted in 10^6 steps (see figures B.1, B.2 and B.3).

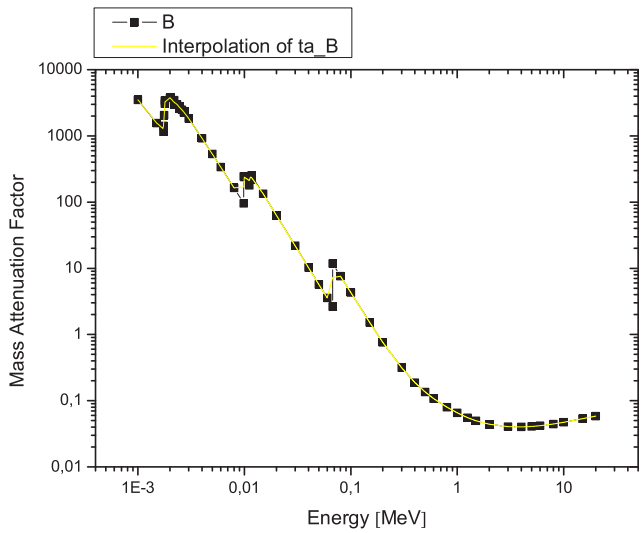

Figure B.1: Plot of the fitted values of the mass absorption coefficients for Ta.

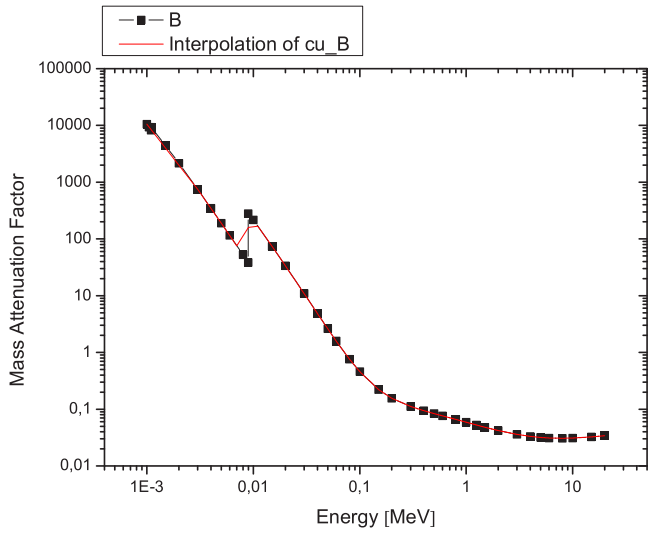

Figure B.2: Plot of the fitted values of the mass absorption coefficients for Cu.

To calculate the overall absorption, the values for each element have been multiplied with each other.
For Ta as backing material we get

$$(I/I_0)^{Ta}_{gesamt} = \left(\frac{I}{I_0}\right)_{Pb} \left(\frac{I}{I_0}\right)_{Ta} \tag{B.3}$$

for Cu as backing material we get

$$(I/I_0)^{Cu}_{gesamt} = \left(\frac{I}{I_0}\right)_{Pb} \left(\frac{I}{I_0}\right)_{Cu} \tag{B.4}$$

Table B.1: An example of the absorptions for the radioactive standard sources are listed. A list of all absorption coefficients would go beyond the scope of this scope.

Source	E_{gamma} (keV)	$(I/I_0)^{Ta}_{gesamt}$	$(I/I_0)^{Cu}_{gesamt}$
^{60}Co	1173.228	0.8428	0.8190
	1332.492	0.8424	0.8328
^{133}Ba	276.4	0.2420	0.2760
	302.85	0.3129	0.3447
	356.01	0.4252	0.4501
	383.84	0.4763	0.4968
^{137}Cs	661.6	0.7167	n.b.

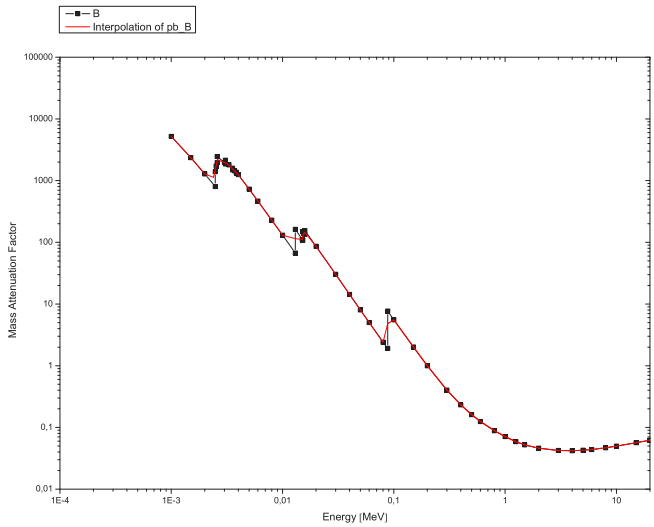

Figure B.3: Plot of the fitted values of the mass absorption coefficients for Pb.

Bibliography

[1] Rolfs C.E. and Rodney W.S., 1974, Nuclear Physics A, 227, p. 291

[2] Wiescher M. , Görres J. and Schatz H., 1999, Nuclear Particle Physics, 25, R133

[3] José J., Coc A. and Hernanz M., 1999, Astrophysical Journal, 520, p. 347

[4] Rowland C., Iliadis C., Champagne A.E., Fox C., José J. and Runkle R., 2004, Astrophysical Journal, 615, L37

[5] Tanner N., 1959, Physical Review, 114, p. 1060

[6] Rolfs C.E., Rodney W.S., Shapiro M.H. and Winkler H., 1975, Nuclear Physics A, 241, p. 460

[7] Stech E., Ph. D. Dissertation, The Astrophyscial Impact of the $^{20}Ne(p,\gamma)^{21}Na$ Reaction, University of Notre Dame, USA

[8] Knoll G., Radiation Detection and Measurement, 3rd edition, 2000, Wiley

[9] Leo W.R., Techniques for Nuclear and Particle Physics Experiments: A How-To Approach, 2nd Rev edition, 1994, Springer

[10] Bellamy E.H. et al., 1967, Physical Review, 164(2), p. 417

[11] Antilla et al., Nuclear Instruments and Methods, 1977, 147, p. 501

[12] Meyer et al., Nuclear Physics A, 1975, 250, p. 235

[13] Endt et al., Nuclear Physics A, 1990, 510, p. 209

[14] Debertin K. und Helmer R.G. , Gamma- and X-Ray spectrometry with semiconductor detectors, 1988, North-Holland

[15] Semkow et al., Nuclear Instruments and Methods in Physics Research, 1990, A290, p.437

Acknowledgments

I would like to thank Prof. Dr. K.-L. Kratz [1], Prof. Dr. M. Wiescher [2] and Prof. Dr. J. Görres [2] , who gave me the opportunity to perform the experiments at the University of Notre Dame.

Emphasis should be given to the support provided by Prof. Dr. J. Görres and Dr. E. Stech, who have been more than helpful with their patience and advice.

Also i would like thank the technical personnel of the Nuclear Structure Laboratory directed by Prof. Dr. L. O. Lamm, who offered help with conditioning and building the technical devices.

Financially this work was supported by HGF VISTARS (Virtuelles Institut der Struktur der Kerne und nuklearer Astrophysik), JINA (Joint Institute of Nuclear Astrophysics) and the University of Notre Dame du Lac, Indiana, USA.

I would thank like Timo Griesel, Shawn O´Brien, Florian Schertz, Ruben Kessler and Paul James LeBlanc IV for the wonderful time during my time at Notre Dame.

At last I like to thank my parents and my brother, without their support I would have not been able to finish my work.

[1] Institut für Kernchemie, Johannes Gutenberg-Universität Mainz, D-55128 Mainz
[2] Department of Physics, University of Notre Dame, Notre Dame, Indiana 46556, USA